ACS APPLIED MATERIALS & INTERFACES

Research Article

www.acsami.org

Selective Dispersion of Highly Pure Large-Diameter Semiconducting Carbon Nanotubes by a Flavin for Thin-Film Transistors

Minsuk Park,[†,§] Somin Kim,[†,§] Hyeokjae Kwon,[‡,§] Sukhyun Hong,[†] Seongil Im,[‡] and Sang-Yong Ju*[,†]

[†]Department of Chemistry and [‡]Department of Physics, Yonsei University, Seoul 03722, Republic of Korea

Supporting Information

ABSTRACT: Scalable and simple methods for selective extraction of pure, semiconducting (s) single-walled carbon nanotubes (SWNTs) is of profound importance for electronic and photovoltaic applications. We report a new, one-step procedure to obtain respective large-diameter s- and metallic (m)-SWNT enrichment purity in excess of 99% and 78%, respectively, via interaction between the aromatic dispersing agent and SWNTs. The approach utilizes *N*-dodecyl isoalloxazine (FC12) as a surfactant in conjunction with sonication and benchtop centrifugation methods. After centrifugation, the supernatant is enriched in s-SWNTs with less carbonaceous impurities, whereas precipitate is enhanced in m-SWNTs. In addition, the use of an increased centrifugal force enhances both the purity and population of larger diameter s-SWNTs. Photoinduced energy transfer from FC12 to SWNTs is facilitated by respective electronic level alignment. Owing to its peculiar photoreduction capability, FC12 can be employed to precipitate SWNTs upon UV irradiation and observe absorption of higher optical transitions of SWNTs. A thin-film transistor prepared from a dispersion of enriched s-SWNTs was fabricated to verify electrical performance of the sorted sample and was observed to display p-type conductance with an average on/off ratio over 10^6 and an average mobility over 10 $cm^2/V{\cdot}s$.

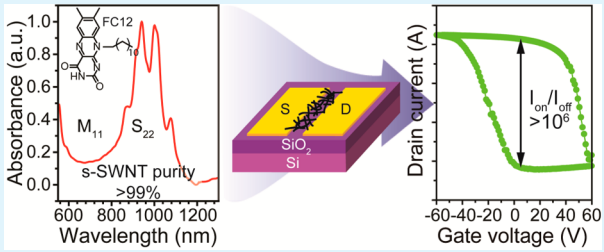

KEYWORDS: *carbon nanotubes, sorting, flavin, photoreduction, field effect transistor*

INTRODUCTION

Semiconducting (s) single-walled carbon nanotubes (SWNTs), cylindrical rolls of graphene sheets defined by a chiral (*n*, *m*) vector, have excellent electrical, mechanical, and optical properties,[1] which make them appropriate for various applications, including high-performance thin-film transistors (TFTs),[2−5] photovoltaics,[6,7] chemosensors,[8] and electronic skins.[9,10] They are processable from solution and are of great interest for flexible electronics.[11−14] However, most SWNT synthetic procedures result in a mixture of s and metallic (m) nanotubes,[15] and m-SWNTs must be completely discarded to prevent shorted failure of electronic devices and to provide homogeneous electronic performance.

For the past two decades, many methods have been explored to enrich pure s-SWNTs. Sorting methods employed for this purpose take advantage of the electronic structures of SWNTs: m-SWNTs have a finite density of states (DOS) of electrons at the Fermi level, while s-species have a bandgap whose band gaps are inversely proportional to SWNT diameter (*d*) or chiral vector sizes.[1] Exploiting intrinsic band structure difference, electrical breakdown[16] and the recently developed thermocapillary enabled etching methods[17,18] attain highly effective removal of m-SWNTs. However, such methods are not easily scalable. Popular large-quantity sorting techniques, e.g., liquid column chromatography (LCC),[4,19,20] density gradient ultracentrifugation (DGU),[21−23] polymer-assisted aqueous two-phase partition (ATP),[24,25] and selective dispersion using conjugated polymers[26−29] typically exploit subtle differences in adsorbed configuration of the dispersing agents on SWNT species which result from different SWNT polarizability. Sorting of smaller *d* tubes such as HiPco (*d*: 0.65−1.35 nm) and CoMoCAT tubes (*d* < 1.0 nm) is much more favorable due to more distinct bandgaps. Using these SWNTs, researchers demonstrate single s-SWNT purity over 94%.[20,30,31] For larger *d* SWNTs, the sorting efficiency is limited by the subtle difference in SWNT bandgap structure.[25,32,33] In order to attain higher purity, multiple iteration or additional SWNT bundle removal steps (DGU[28]) are required. A novel class of sorting mechanism that directly exploits the band structure difference between s- and m-SWNTs may likely achieve much higher sorting efficiency.

However, no work has been reported that can realize high-purity s-SWNT sorting by utilizing discrete highest-occupied molecular orbital (HOMO) and lowest-unoccupied molecular orbital (LUMO) of dispersing agents in conjunction with band structure of m- vs s-SWNTs. The closest analogue for this method is ATP-based separation which utilizes different oxidation depth of SWNTs according to electronic types and partitions them in different media.[34] In this aspect, *N*-dodecyl isoalloxazine (FC12, inset of Figure 1)[35,36] is capable of dispersing SWNTs in nonpolar aromatic solvents by a process involving helical wrapping. The SWNTs generated in this way have sharp absorption features and nearly no background

Received: June 9, 2016
Accepted: August 19, 2016
Published: August 19, 2016

DOI: 10.1021/acsami.6b06932
ACS Appl. Mater. Interfaces 2016, 8, 23270−23280

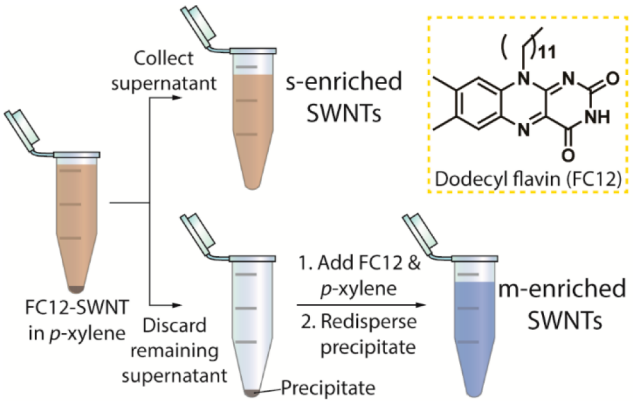

Figure 1. Outline of facile s- and m-SWNT enrichment process. Inset: chemical structure of FC12.

absorption characteristics originating from carbonaceous impurity. Recently, FC12 was utilized to separate s-SWNTs in smaller *d*, confirmed by Raman spectroscopy with single laser excitation.[37] However, FC12 absorption screening m-SWNT absorptions hampers accurate estimation of purity. Highly pure s-SWNT separation will be a facile venue to deploy s-SWNTs for various high-end optoelectronic applications.

In the investigation described below, we developed a method for facile enrichment of s- and m-SWNTs having energy transfer from FC12 to SWNTs. In this system, in which FC12 is employed as a dispersing agent, enrichment is performed simply by collecting a supernatant and precipitate after facile benchtop centrifugation. Owing to the high individualization and dispersion, a one-step FC12-SWNT dispersion in *p*-xylene can be separated selectively to give highly pure s-SWNT with over 99.5% purity in the supernatant and 78% pure m-enriched SWNT in the precipitate, based on absorption measurements. Moreover, the use of elevated mild centrifugal force can achieve higher purity of the larger *d* s-SWNT. Photoluminescence (PL) along with absorption spectrum suggest that energy transfer from FC12 to SWNTs is facilitated, leading to SWNT PL increase. In addition, the photoreduction properties of FC12 can be used advantageously to precipitate SWNTs. The result of this property enables generation of a SWNT that can be probed using the entire UV−vis absorption range. Finally, s-enriched SWNT, prepared in the manner described above, was utilized to verify electronic performance by preparing a p-type random network SWNT TFT[38] and shows current on/off ratio above 10^6 and mobility exceeding 15 $cm^2/V{\cdot}s$.

RESULTS AND DISCUSSION

FC12 was synthesized by using a previously reported method.[36] Owing to the 550 nm absorption tail of FC12, plasma torch-grown SWNT (PSWNT, *d* distribution: 1.3 ± 0.4 nm) was initially used in this experiment. FC12-PSWNT dispersions in *p*-xylene were generated by using FC12 as a surfactant via a probe sonication. For comparison purposes, sodium dodecyl sulfate (SDS)-PSWNT dispersions[39−41] were prepared in water (see Experimental Section for detailed procedures).

A schematic of the procedure used to enrich s- and m-SWNT from a SWNT mixture is given in Figure 1. In contrast to the centrifugation speed used for separation of SDS-SWNT samples in water (80 000*g*), a much slower benchtop centrifugation speed (5000*g*) leads to profound enrichment of s- and m-SWNTs prepared using FC12 (see below). After benchtop centrifugation, high purity s-SWNTs are present in the supernatant, whereas redispersion of the remaining precipitate in *p*-xylene containing additional FC12 produces a m-enriched SWNT dispersion, suggesting s-PSWNT selectivity.

In Figure 2a are shown absorption spectra of the supernatant and precipitate of centrifuged FC12-PSWNT dispersions along

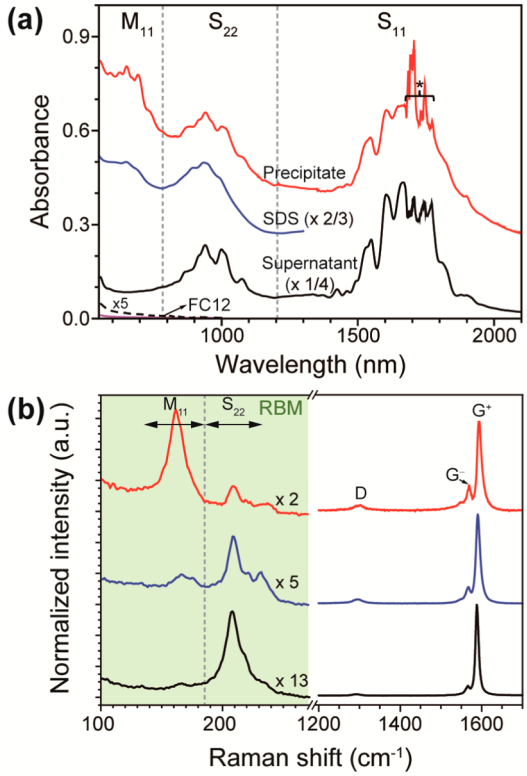

Figure 2. Enrichment of s- and m-PSWNTs dispersed by FC12. (a) Absorption spectra of supernatant (black) and precipitate (red) of FC12-PSWNT, along with that of supernatant (blue) of SDS-PSWNT. Residual FC12 absorption tail (dotted line) having same concentration of the dispersion is magnified on top of the initial spectrum (magenta). It is noteworthy that the spectra are nonoffset. An asterisk indicates the absorption attributed to *p*-xylene. (b) Raman RBM and G band spectra of PSWNT on 285 nm thick SiO_2/Si substrate, excited by using a 785 nm laser. The spectra are shifted vertically for visual clarity. A double arrow indicates resonating windows of M_{11} and S_{22} peaks for a given PSWNT *d* range. Dotted line designates median *d*.

with that produced from aqueous SDS-SWNT dispersion. In the absorption range of 550−2100 nm, SWNTs display absorption caused by one m- (570−800 nm) and two s-optical transitions (800−1200 nm, 1200−1900 nm), which are indicated by M_{ii} and S_{ii} (ii denotes optical transitions), respectively. Absorption bands in the spectra are associated with the individual nanotube species (*n*, *m*) present in each. In contrast to the broadly featured absorption spectrum (blue trace) of SDS-PSWNT, the spectrum of the FC12-PSWNT supernatant (black) contains sharper and intense S_{11} and S_{22} peaks and nearly no M_{11} peaks. In addition, despite the high impurity content of PSWNT (30 to 70%), background absorption of the supernatant is small. This result suggests that the use of FC12 leads to selective formation of s-SWNTs over background absorption contributors such as π-plasmon and carbonaceous impurities. This demonstrates that highly pure s-enriched SWNTs are present in the FC12-PSWNT supernatant. As a result, the peaks observed in absorbance can easily be assigned to (*n*, *m*) nanotubes seen in photo-

DOI: 10.1021/acsami.6b06932
ACS Appl. Mater. Interfaces 2016, 8, 23270−23280

luminescence excitation (PLE) maps (see Figure S1a of Supporting Information (SI)). Eight major PL peaks are observed from FC12-PSWNTs, and their positions are listed in Table S1 of SI. PLs of PSWNTs having *d* values ranging from 1.1 to 1.28 nm were observed, rather than up to 1.7 nm due to both overtone (1600 to 1830 nm) of C−H stretch bands of *p*-xylene methyl moieties and detection limit (<1650 nm) of InGaAs array detector used in the PLE setup. The PLE map includes PSWNTs that have various chiral angles and does not show substantial chirality-specific selectivity which is observed in the near-armchair s-SWNT enrichment obtained using a polyfluorene-SWNT toluene dispersion.[26] In this sense, the less specificity of FC12 in generating certain s-SWNT chiralities serves advantageously for bulk sorting of s-/m-SWNT. The FC12-assisted PSWNT dispersion is stable under a dark condition at least for a year without visible aggregation or significant reduction or broadening in UV−vis−NIR absorption spectra (Figure S2a−c).

The spectrum of the precipitate contains M_{11} and S_{22} bands with nearly equal intensities. Especially, the band for M_{11} in the precipitate is significantly larger than that of SDS-PSWNT. Although the spectra appear to show similar abundances of m- and s-contents in the precipitate, actually there is a greater amount of m-enriched SWNTs because higher-order optical transitions of SWNTs have progressively smaller absorption cross sections.[42]

Raman spectroscopy is used to confirm the purities of s- and m-SWNT. Specifically, the radial breathing mode (RBM) of SWNTs was used to determine SWNT *d*.[43,44] In Figure 2b are shown RBM spectra (785 nm excitation) of PSWNTs derived from the procedure (see Experimental Section for details). In accordance with previous studies,[4] analysis of the experimental Kataura plot[45] (see SI for detailed RBM analysis) showed that resonating regions of m- and s-PSWNT exist with 785 nm. On the contrary to results obtained in studies of supernatants (black) where the S_{22} peak areas are greater than those of the M_{11} counterparts, the spectra of the precipitates show the opposite trend. A comparison of RBM peak areas in the spectra of m- and s-SWNTs enables an estimate of s- and m-PSWNT purities to be 95 and 78%, respectively. This Raman result is in good agreement with the absorption-based enrichment. It is noteworthy that the 785 nm laser probes both smaller *d* s- and larger *d* m-PSWNTs, and this assessment may reflect only a small fraction of PSWNTs, in resonance with a given laser. The corresponding high frequency regions show G^+, G^-, and D bands at ca. 1590, 1566, and 1300 cm^{-1}, respectively. m-Enriched precipitates exhibit slightly broadened G^- band spectra as compared to that of s-enriched supernatant, suggesting the inclusion of Breit−Wigner−Fano (BWF) resonance of m-SWNT.[46] In addition, comparison of D and G bands from each sample suggests that D over G band ratio (I_D/I_G) of precipitate (0.06) is six times higher than that (0.01) of the supernatant, probably due to sp^3-type defects from prolonged sonication time (2 vs 1 h) and inclusion of carbonaceous impurity. It is noteworthy that Raman spectra of the as-supplied PSWNT dispersed in acetone with a brief 1 min sonication show larger I_D/I_G (0.03) than that from the s-enriched PSWNT (Figure S3). This ratio suggests that the s-PSWNT portion has lower defect density than that of the initial dispersion by excluding carbonaceous impurity, in line with the observed s-enriched absorption spectra with lower background absorption.

Semiconductor purities of supernatants can be enhanced by using a greater benchtop centrifugal force. In Figure 3a are shown absorption spectra of the supernatants obtained from using an

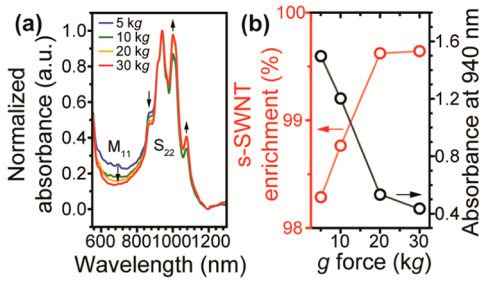

Figure 3. (a) 940 nm normalized absorption spectra of FC12-PSWNT dispersions as a function of centrifugal force. (b) The corresponding absorption-based s-SWNT enrichment and absorbance change at 940 nm.

increasing *g*-force (5, 10, 20, and 30 kg). Although the overall absolute S_{22} absorption decreases as the *g*-force increases (Figure 3b), the M_{11} one decreases much more rapidly. Inspection of background-subtracted absorption spectra normalized to the 940 nm peak (see Figure S4b of SI) clearly shows that the M_{11} peaks decrease as the centrifugal force increases. Moreover, increased *g*-force selects for larger *d* s-SWNTs (marked by arrows in Figure 3a). Comparison of the corresponding PLE maps of these samples (see Figure S1a−d of the SI) demonstrates that s-SWNTs with smaller *d* (i.e., (13,2) and (12,4)) decrease, and larger *d* s-SWNTs (i.e., (13,5)) slightly increase with increasing *g*-forces. The reason for larger *d* PSWNT selection of FC12 with increased *g* force originates from larger binding energy of the isoalloxazine moiety of FC12.[47] Moreover, this is in good agreement with our recent result that flavin is an efficient dispersing agent to disperse graphene, an infinite version of large *d* SWNTs.[48] This finding suggests that FC12 has the propensity to generate slightly larger *d* s-SWNTs at high centrifugal force.

In order to quantify the purities of m- and s-SWNTs, the widely used absorption based purity[4,23,28,29,49] by using S_{22} and M_{11} peak areas was utilized. Because the SDS surfactant (blue trace of Figure 2a) leads to no selectivity in the generation of SWNT electronic types, normalizing the background-subtracted FC12-SWNT absorption to that of SDS-SWNT and assuming the existence of a 2 s-/m-ratio gives an absorption-based estimate of s- and m-SWNT purities (see SI for the detailed calculation procedure and Table S2). Figure 3b shows the trend in s-enrichment of the supernatant with increasing *g*-force. The supernatant produced using 5000 *g* shows ca. 98.3% enrichment. The use of increasing *g*-force with 20 and 30 kg further elevates the absorption-based purity to over 99.6%. It is noteworthy that inclusion of background absorption contribution would lower the estimated purities. This result obtained by benchtop centrifugation contrasts with those using the s-SWNT enrichment method based on over 100 kg ultracentrifugation[50,51] and demonstrates effective control of s-SWNT purity.

Moreover, we determined the s-PSWNT yields from each sample. Here, s-PSWNT yield is defined as isolated mass of s-PSWNTs relative to the initial s-PSWNTs in the starting material. In order to measure isolated s-PSWNT yield, the s-PSWNT film was prepared after the photoreducing FC12 in s-enriched supernatant to be discussed in a later section, followed by filtration and a copious washing step with methanol to remove excess FC12 (see Experimental Section for details). Since the PSWNT film may contain adsorbed photoreduced FC12, the vacuum-annealed sample was subject to thermogravimetric analysis (TGA) (Figure S5). Comparison of TGA traces shows that about 47 wt % of the photoreduced FC12-PSWNTs

DOI: 10.1021/acsami.6b06932
ACS Appl. Mater. Interfaces 2016, 8, 23270−23280

originates from PSWNTs. Based on the TGA-determined isolated PSWNT contents and consideration of supernatant amount and initial semiconductor abundance in a quoted PSWNT purity, the isolation yield is about 13% in a single extraction, which is nearly half the recent 22% isolation yield of s-enriched PSWNTs.[29] Using the measured absorbance relationship in Figure 3b, the yields of other s-enriched samples are listed in Table S2.

Analysis of a HiPco nanotube, which has a smaller median *d* (1.0 nm) than PSWNT does, suggests that the use of FC12 lowers the selectivity and dispersion for smaller *d* tubes. In Figure 4a are shown absorption spectra of the supernatant and

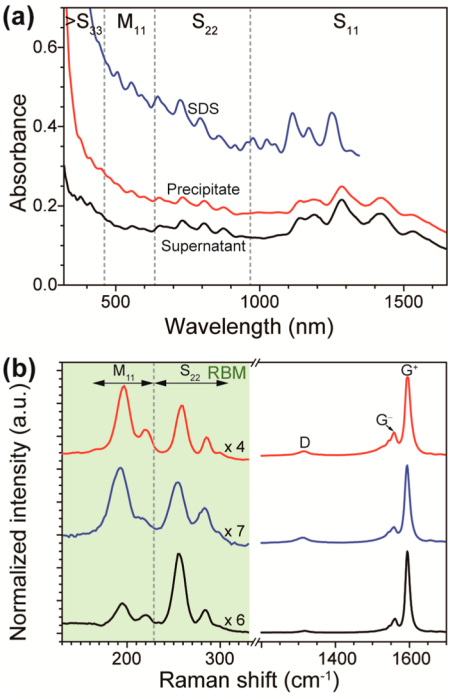

Figure 4. Electronic enrichment of supernatant and precipitate from FC12-HiPco dispersion samples. (a) Absorption spectra of FC12-removed HiPco in NMP and (b) RBM, D, and G band spectra of HiPco on 285 nm thick SiO_2/Si substrate, excited by 632.8 nm laser. Black, red, and blue traces denote supernatant, precipitate of FC12-HiPco dispersions, and supernatant of SDS-HiPco, respectively. Raman spectra were shifted vertically for clarity. Double arrow indicates resonating M_{11} and S_{22} peaks with a given excitation. Dotted line designates median diameter.

precipitate of FC12-HiPco dispersions, which are redispersed in *N*-methyl-2-pyrrolidone (NMP) by using solvent exchange (see Experimental Section for details), along with that from aqueous SDS-HiPco dispersion. Solvent exchange was achieved after photoreduction of FC12 (see below). Because FC12 is completely photoreduced, the full absorption range up to 300 nm can be probed. The M_{11} region (440−600 nm) of this dispersion was compared with those of S_{22} and S_{11} of HiPco samples. Unlike the clear trend observed in larger *d* PSWNTs, the supernatant shows smaller M_{11} peaks as compared to those of S_{22} peaks, and the precipitate displays the opposite trend. Moreover, absorptivities of the supernatant and precipitate from the smaller *d* HiPco sample are much lesser than those (Figure 2a) from the larger *d* PSWNT sample. This suggests that FC12 has less dispersion with smaller *d* SWNT, in line with a previous report.[37]

Since the HiPco tube has partially overlapped M_{11} and S_{22} absorption peaks,[52] purities of the supernatant and precipitate were estimated by using Raman analysis. Left of Figure 4b displays RBM spectra (632.8 nm excitation)[4] of HiPco from each sample (see Experimental Section). The s-and m-SWNT purities of supernatant and precipitate were found to be 76 and 61%, respectively. Along with the trends seen in the centrifugation studies, this result gives further evidence to the conclusion that the use of FC12 leads to selective production of larger s-nanotubes. The I_D/I_G ratio from Raman spectra (right of Figure 4b) follows similar trends observed for PSWNT, showing the smallest value for the supernatant sample as compared to that of the precipitate.

We find that the FC12 promotes the occurrence of energy transfer between the SWNT and isoalloxazine. Evidence supporting this proposal was acquired by analysis and comparisons of absorption and PL spectra of FC12 and the PLE maps of FC12-HiPco and FC12-PSWNT with excitation in the range of 350−900 nm (Figure 5a−c). Interestingly, strong PL emissions at the absorption (400−500 nm) of FC12 are present in the PLE maps of both FC12-HiPco and PSWNT, and the PL emission positions stem from S_{11} of each SWNT. This observation indicates that energy transfer from excited FC12 to s-SWNTs occurs. Thus, the photon energy absorbed by FC12 is transferred to the state corresponding to the S_{22} band of SWNT, which then internally relaxes to the state responsible for the S_{11} band, from which the emissions take place. A similar type of energy transfer process has been observed in polyfluorene-SWNT[53] and organic dye-encased SWNT[54] systems. In the FC12 system, the energy transfer process seems to be facilitated by close proximity (0.34 nm) of the SWNT and the surfactant, which is helically wrapped around the SWNT owing to $\pi-\pi$ interactions.[35] Since Coulombic coupling of the equally longitudinal transition dipoles of both the isoalloxazine chromophore in FC12[55] and the SWNTs[56] is the basis for the energy transfer process,[57] the spectral overlap could strengthen binding, as evident by the pyrene excimer which shows larger binding affinity as large as 0.4 eV.[58] As a result, the photoinduced energy transfer facilitates red-shifted SWNT PL by 15−51 and 23−71 meV in S_{11} and S_{22}, respectively, as compared to those of SDS-SWNT.[35,36]

Figure 5d illustrates the energy diagram of isoalloxazine moiety, HiPco, and PSWNT. HOMO and LUMO of isoalloxazine are −6.4 and −3.5 eV,[59] respectively, and Fermi level of SWNTs is at ca. −4.7 eV.[60] Such energy level alignment facilitates the aforementioned energy transfer from the excited FC12 to both SWNT types. In the ground state, on the other hand, SWNT leads to a charge transfer to FC12, which is evident by theoretical calculation[61] and electrochemical measurement.[62]

The photoreduction capability of FC12 was utilized advantageously to control the dispersion and induce precipitation of the SWNTs. Upon photoirradiation, flavins are known to undergo reduction to form their reduced dihydro-states (FlavinH_2, Figure 6a). These reduced forms can be converted back to their oxidized state counterparts by molecular oxygen.[63] Upon reduction, the isoalloxazine ring in FC12 undergoes a profound conformational change to generate a bent form (bottom panel of Figure 6a).[64−66] Importantly, FC12 reduction causes a large change in UV−vis absorption and luminescence characteristics of FC12.[35,61] Using this photochemical phenomenon, we were able to induce SWNT precipitation and reduction of FC12 absorption and PL. The formation of photoreduced FC12-H_2 in the photoreduced mixture was demonstrated by

DOI: 10.1021/acsami.6b06932
ACS Appl. Mater. Interfaces 2016, 8, 23270−23280

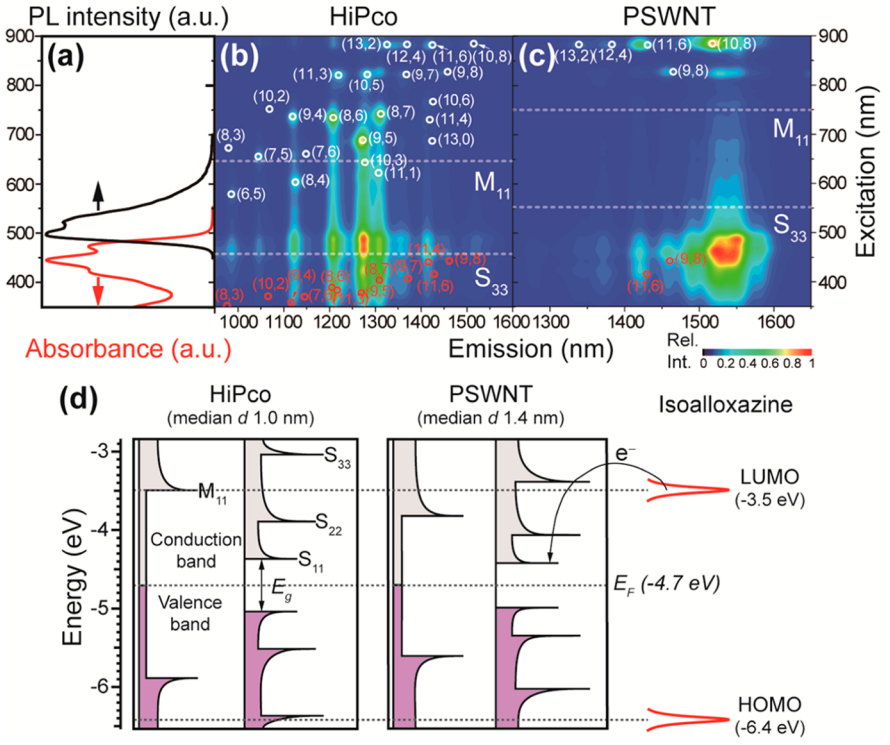

Figure 5. Energy transfer from FC12 absorption to SWNTs. (a) absorption (red) and PL (black) spectra of FC12 only. Excitation: 445 nm. PLE map of (b) FC12-HiPco and (c) FC12-PSWNT. Dotted line indicates boundary of electronic types. (d) Energy diagram of isoalloxazine and SWNTs.

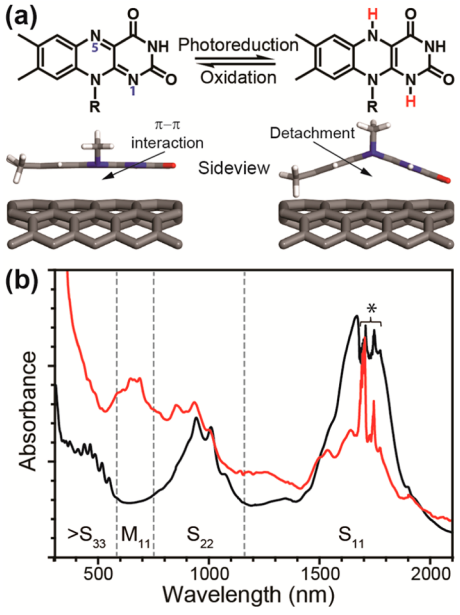

Figure 6. Photoreduction of FC12 and subsequent surfactant-absorption-free, PSWNT absorption spectra in NMP. (a) Photoreduction of planar FC12 produces bent FC12-H_2. A side view of the reduced form shows that $\pi-\pi$ interactions are lost. (b) Absorption spectrum of FC12-depleted SWNT while stirring. Supernatant (black) and precipitate (red) of PSWNT. An asterisk indicates the absorption attributed to residual *p*-xylene.

using liquid chromatography (LC)-mass (MS) spectroscopy (see Figure S6a–d of the SI and Experimental Section for details). In the mass spectrum of the photoreaction mixture, a peak was present at m/z = 413.26 ($[M + H]^+$), which corresponds to reduced and protonated FC12 species. The results show that photoreduction-induced changes in the electronic properties of surfactants can serve as the basis for designing novel methods to promote SWNT precipitation. The evidence that reduced FC12 still exists on the SWNT sidewall is obtained from the aforementioned TGA result in Figure S5, supporting the right scheme of Figure 6a.

By using the new method in which FC12 absorption does not occur, SWNTs can be easily transferred to neat NMP for optical measurements. In Figure 6b are shown absorption spectra of the supernatant and precipitate of 5000 *g* FC12-depleted PSWNTs, recorded while the solution was mechanically stirred. The spectra contain absorptions arising from transitions greater than S_{33}, along with a slightly broadening and red-shifting of S_{22} peaks due to SWNT bundling (see Figure S7 for comparison). As compared to that of the initial 5000 *g* dispersion, M_{11} regions of the absorption spectrum of FC12-depleted PSWNTs are more suppressed. The reason for the decrease originates from the absence of an FC12 absorption tail (see absorption spectrum in Figure 2a), along with possible redistribution of PSWNT electronic types in NMP. Further comparison of those spectra with that of an additional reference SWNT sample (magenta) with a known composition (99% s-enrichment) confirms the aforementioned s-enrichment purity in the absence of FC12 contribution.

Prior to electrical measurement, we characterize the length and density of sorted s-PSWNTs from 5000 *g* sample by atomic force microscopy (AFM). The SWNT sample for AFM measurement was prepared via a similar condition for device fabrication. A 5000 *g* sample of the s-enriched supernatant solution was dropcast on mica, followed by repeated washing with methanol and subsequent air-annealing at 250 °C for 1 h, to remove residual FC12. In Figure 7a and b are shown AFM images of the resulting deposited PSWNTs. Large area height image of PSWNT (Figure 7a) exhibits a dense SWNT network with less

DOI: 10.1021/acsami.6b06932
ACS Appl. Mater. Interfaces 2016, 8, 23270−23280

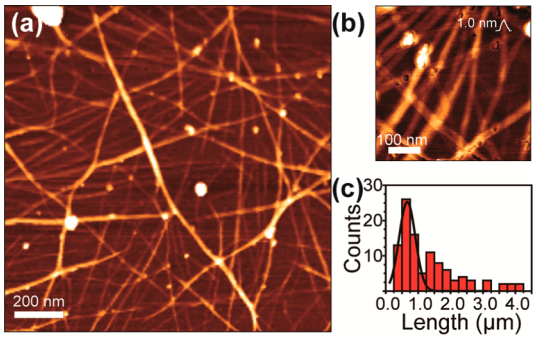

Figure 7. AFM height topographies of the annealed PSWNT on mica. (a) Large area height image of sorted s-PSWNT. (b) Zoomed-in image of PSWNT with height profile. (c) Length histogram of s-PSWNT.

carbonaceous impurities. The measured tube density is ca. 52 tubes/μm^2. This density is much higher than that of SWNTs assembled on an amine-functionalized Si substrate.[50] Zoomed-in image of PSWNT (Figure 7b) provides a height profile of an individual tube, showing 1.0 nm. Considering d distribution of PSWNTs (1.3 ± 0.4 nm) along with two van der Waals (vdW) distances (2 × 0.34 nm) between FC12 and PSWNTs,[35] such tube height suggests that FC12 around PSWNTs is effectively eliminated, due to the 1 h annealing process. Moreover, the smooth tube surface suggests lack of FC12 helical wrapping on the SWNT which was observed in a flavin-wrapped SWNT in our previous work.[35,67] Figure 7c displays the length histogram of PSWNTs and shows the median length of PSWNTs to be 0.66 ± 0.05 μm, obtained by analyzing 104 tubes of the 5000 g sample.

Moreover, the spatial homogeneity of purity of the deposited s-PSWNT on a substrate was probed by Raman mapping with 532 nm excitation (see SI for the detailed explanation). Figure S8a and b displays RBM and G band spectra from nearly 2500 different points. The RBM spectra display prominent peaks at 174 and 185 cm^{-1}, corresponding to s-PSWNT species whose d are 1.36 and 1.27 nm, with nearly no m-PSWNT signal except the residual tailing of s-PSWNT peaks. The corresponding G band displays narrow G^- and G^+ bands at ca. 1568 and 1594 cm^{-1}. The absence of a broad BWF G^- component substantiates preferential enrichment of s-PSWNT mentioned in the above discussion. Spatial maps according to RBM regions and G band regions confirm homogeneous SWNT electronic-type distribution upon substrate deposition.

The electrical performance capability of the s-SWNT, as obtained by using the sorted s- and m-PSWNT sample at 5000 g described above, was demonstrated by incorporating it in a back gate TFT device. The defined channel length (L) and width (W) are 300 and 20 μm, respectively, as shown in the inset of Figure 8a. A 5000 g s-enriched PSWNT sample was dropcast and treated as mentioned above. An area other than the electrode and channel was oxygen-plasma cleaned to remove the possibility of current leakage through nonchannel pathways. A 50 nm thick layer of Al_2O_3 was atomic-layer deposited over the SWNT channel to provide high dielectric passivation (Figure 8b). In order to confirm that SWNT still possesses random network structure on the SiO_2/Si substrate, we resorted to scanning electron microscopy[19] which allows us to image SWNTs through the Al_2O_3 layer. Figure S9a,b of the SI revealed that individualized SWNTs are densely percolated, and their density is about 15 tubes/μm^2, slightly lower than that of AFM measurement on mica. This suggests that substrate affects SWNT density significantly.

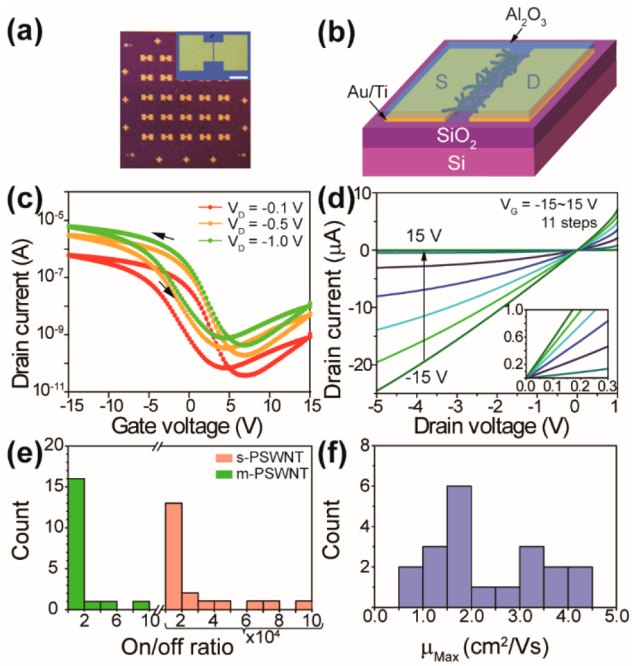

Figure 8. Device performance of s-enriched PSWNT obtained from a 5000 g sample. (a) Picture of TFT array. Inset: optical microscope image of an individual TFT device. Scale bar: 250 μm. (b) Schematics of back gate TFT device. (c) I_D–V_G transfer characteristics measured at different V_D. (d) I_D–V_D output characteristic at different V_G. (e) I_{on}/I_{off} ratio histogram from s-/m-enriched PSWNT devices. (f) Mobility histogram from s-PSWNT devices.

In Figure 8c are displayed the drain current–gate voltage (I_D–V_G) transfer characteristics of the TFT device as measured by using a semiconductor parameter analyzer. The device shows p-type conduction with high current on/off ratios over ~10^4 at each different drain voltage (V_D). As compared to the large hysteresis of the device without Al_2O_3 deposition (Figure S10), this device displays similar forward and backward curves, suggesting that Al_2O_3 passivation on the SWNT device effectively passivates possible charge trap sites on SWNTs. These transfer characteristics contrast starkly with that prepared by 78% enriched m-PSWNT, whose on/off ratio is substantially less than 10, as shown in Figure S11a of the SI. The linear mobility (μ_{lin}) of the s-PSWNT device was estimated using the following equations, trans-conductance g_m (V_G) = dI_D/dV_G and $\mu_{lin} = (g_m/C_{ox}V_D) \times (L/W)$, where C_{ox} and V_D are the dielectric capacitance of SiO_2 ($C_{ox} = 1.21 \times 10^{-8}$ F/cm^2) and drain voltage, respectively. The maximum mobility (μ_{max}) was determined to be 4.2 cm^2/V·s. The I_D–V_D output characteristics (Figure 8d) of the devices show that ohmic contact exists between the SWNT and Au/Ti electrodes. A total of 39 devices from each supernatant/precipitate sample were prepared, and statistics of on/off current ratio and μ_{max} value were obtained (Figure 8e and f). The average on/off ratio of s-enriched and m-enriched PSWNT devices shows an average of 2.7 × 10^4 and 1.9, respectively, which are similar to those of TFT devices prepared by 94% s-enriched SWNT by using an agarose gel purification.[4] Average μ_{max} of s-enriched PSWNT devices displays 2.3 cm^2/V·s.

We further improve a device performance by using 30 kg s-enriched SWNT via dipcoating method, as illustrated in Figure 9a. The fact that higher centrifugation results in purer s-PSWNT dispersion infers that dropcasting might induce preferential m-PSWNT precipitation in the device. The inset of Figure 9a

DOI: 10.1021/acsami.6b06932
ACS Appl. Mater. Interfaces 2016, 8, 23270–23280

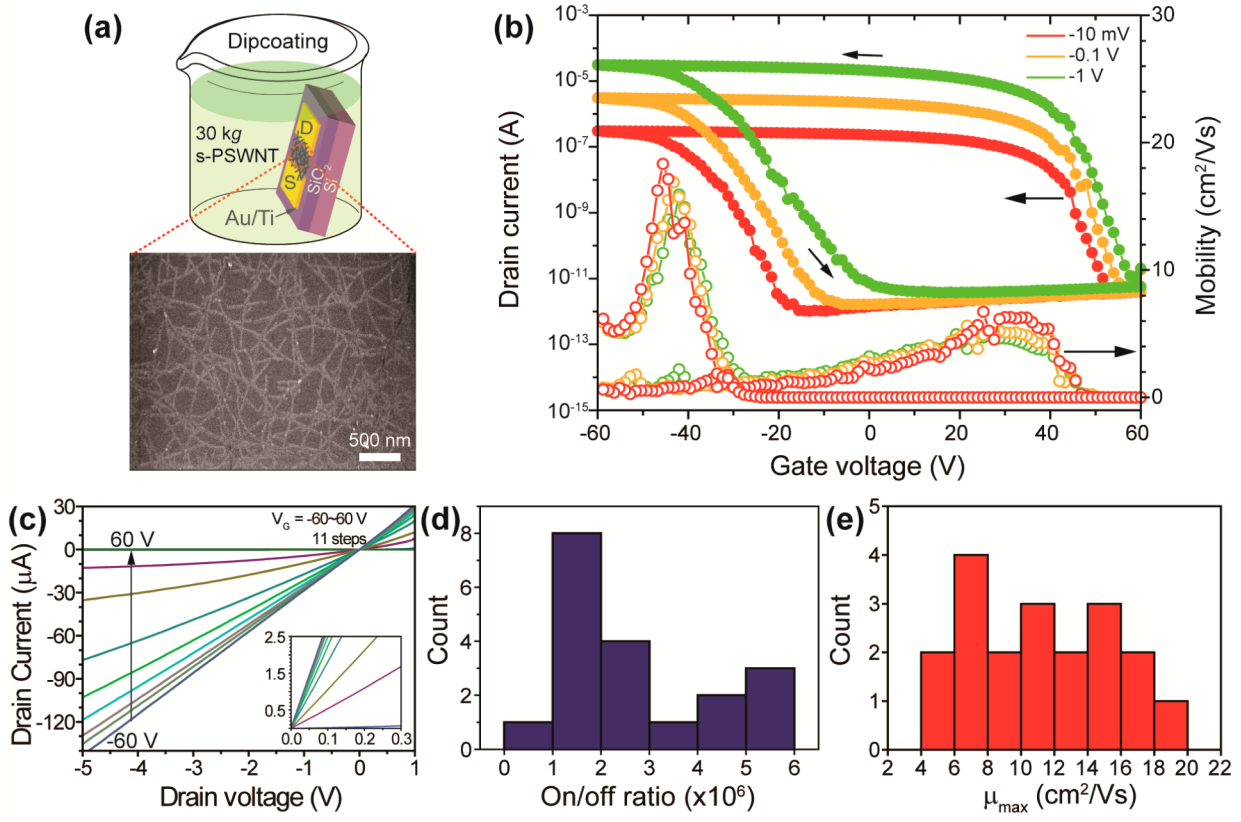

Figure 9. Device performance of s-enriched PSWNT obtained from a 30 kg sample via dipcoating. (a) Dipcoating of a prepatterned Si substrate into 30 kg s-PSWNT dispersion. Inset: a SEM image of random network PSWNT between device channel. (b) I_D-V_G transfer characteristics (solid circle) and μ_{lin} (empty circle) measured at different V_D. (c) I_D-V_D output characteristic at different V_G. (d) I_{on}/I_{off} ratio and (e) mobility histograms.

displays an SEM image of random network thin film of PSWNTs formed by 1 h dipcoating. The measured nanotube density (15 tubes/μm^2) and morphology remain similar to that of the dropcast sample of 5 kg s-PWNTs (Figure S9). In this time, we prepare TFT devices without Al_2O_3 deposition. Although the absence of Al_2O_3 passivation layer results in hysteresis, the resulting representative device (Figure 9b) displays p-type conductance behavior with high current on/off ratio and μ_{lin} as large as 5.5×10^6 and 18 $cm^2/V{\cdot}s$, respectively. This confirms that s-enriched purity dominantly controls the device performance. The I_D-V_D output characteristics (Figure 9c) of the devices confirm the ohmic contact, observed in the device from the 5 kg sample. A total of 19 devices shows an average on/off current ratio of 2.7×10^6 and an average μ_{max} value of 11.5 $cm^2/V{\cdot}s$ (Figure 9d and e), respectively, which are 2 orders of magnitude and five times higher than those from the device derived from 5 kg, respectively. Interestingly, the 19 devices display uniform current on/off ratio at the level of 10^6 which seems to originate from sample homogeneity enhanced by usage of a 30 kg s-enriched sample and dipcoating method. The mobility varied from 5 to 20 $cm^2/V{\cdot}s$. Overall, the device performances of s-enriched PSWNT mentioned above are similar to those of highly dense TFT SWNT devices prepared by poly(fluorine) sorting.[33]

Our findings provide a more effective way to sort SWNTs by electronic type. Both LCC and DGU require sophisticated instrumentation to employ after dispersion. Our method, on the other hand, is simple and fast, energy-saving, and requires no major instrumentation. Moreover, unlike the polymeric dispersing agent, the small molecular isoalloxazine has no concerns on polymer entanglement-related lowering of SWNT purity.[50] These advantages make our method especially suited for multistep sorting to obtain ultrapure s-tubes.

CONCLUSION

In the investigation described above, we have demonstrated that the organic surfactant FC12 can be used to enrich high purity s- and m-SWNTs in a *p*-xylene simple, affordable, and efficient manner. The method, which does not require preseparation steps and utilizes simple benchtop centrifugation, results in s- and m-SWNTs having purities greater than 99 and 78%, respectively. The resulting s-enriched SWNT displays sharp optical absorption bands along with suppressed background absorption. The use of higher *g*-force in the centrifugation process increases purity of the s-SWNT in excess of 99.6%. FC12 displays a selectivity toward larger s-SWNTs and energy transfer with SWNTs. After its use in the electronic sorting process, FC12 can be eliminated by taking advantage of its ability to undergo photoreduction to form a dihydro-product that binds less tightly to the SWNT. Random network SWNT TFT devices, constructed using SWNTs obtained employing the new procedure, have p-type conductance with a high average current on/off ratio over 10^6 and an average mobility exceeding 10 $cm^2/(V\ s)$. We provide underlying photoinduced energy transfer of aromatic surfactant interacting with SWNTs. Precipitation of SWNTs via the FC12 photoreduction might find a way to position SWNTs in a specific location. Fine tuning of SWNT enrichment protocol along with device geometry modifications would provide a better TFT device performance.

DOI: 10.1021/acsami.6b06932
ACS Appl. Mater. Interfaces 2016, 8, 23270−23280

EXPERIMENTAL SECTION

Materials and Methods. FC12 was synthesized via two steps by using a previously reported method.[36] SDS (I0352) was purchased from TCI. FMN was obtained from Sigma-Aldrich. All solvents are reagent grade and used without further purification. PSWNTs (RN-220 SWNTs, batch# R26-036, length distribution: 0.5−4 μm, SWNT content: 30−70%, *d* distribution: 1.3 ± 0.4 nm) and HiPco SWNTs (Batch #: R1-831, SWNT content >65%, *d* distribution: 1.0 ± 0.35 nm)[68] were purchased from Nanointegris. UV−vis−NIR absorption spectra were acquired using a JASCO V-770 with a cuvette having 1 cm path length. Prior to Raman and AFM measurements, 285 nm thick SiO_2/Si substrate pieces (Lot#7400383-603-Z, Shinetsu, Japan) were cleaned by immersing them in piranha solution (H_2SO_4:H_2O_2 = 7:3) for 20 min and subsequent washing by flow of Milli-Q quality water for 5 min. The substrates were dried with a N_2 stream and were further dried in a vacuum oven at 110 °C for 1 h. TGA was conducted by SDT Q600 (TA Instruments) under N_2 atmosphere from room temperature to 900 °C with ramping rate of 5 °C/min. SEM measurements were acquired by JSM-7001F (JEOL Ltd.) with 10 kV acceleration.

SWNT Dispersions. *s-SWNT Enrichment Based on FC12.* A mixture of 1 mg of SWNT and 1 mg of FC12 was added to 4 mL of *p*-xylene. The resulting mixture was exposed to brief (5 min) bath sonication (Branson 1510 sonicator, 70 W) and further subjected to 1 h tip sonication [40% power (18.8 W/mL), probe tip diameter: 13 mm, VCX 750, Sonics & Materials], cooled with a water circulator maintained at 10 °C. After varying centrifugation steps (i.e., 5000, 10 000, 20 000, and 30 000 *g*, no. 1 fixed-angle rotor, Supra 22K, Hanil or Wisespin CF-10, Daihan Scientific Co., Ltd.) for 2 h, 80% supernatant was collected.

m-SWNT Enrichment. After discarding the residual supernatant, fresh 4 mg of FC12 in 4 mL of *p*-xylene was added to the microcentrifuge tube containing the precipitate. The resulting mixture was tip-sonicated for 1 h at room temperature to produce an m-enriched sample without further centrifugation.

SDS−SWNT Dispersions. A mixture of 1 mg of SWNT and 10 mg of SDS was added to 10 mL of water. The heterogeneous solution was subject to 1 h bath sonication and 4 h tip sonication at 300 W. A 10 h centrifugation at 80 000 *g* (70Ti rotor, Beckman Coulter) was applied. The 80% supernatant was collected to remove SWNT bundles and carbonaceous and metallic impurities. Prior to measurement, the pH of the dispersion was adjusted to 10.

PLE Measurements. PLE spectroscopy measurements were conducted on a Spex Nanolog 3-211 spectrofluorometer (Horiba Jobin-Yvon) excited using a broadband 450 W Xe lamp, equipped with a liquid nitrogen-cooled, multichannel InGaAs array detector (512 × 1 pixel with a detection range of 800−1650 nm) which can detect SWNT PL up to ca. 1.3 nm *d*. A 150 g/mm grating was utilized to disperse the emission light. Excitation and emission slit widths were 14 and 10 nm, respectively. Both excitation and emission light intensities were corrected against instrumental variations using a sensitivity correction factor to produce a PLE map. PL chirality assignments of s-SWNTs were based on PL pattern matching of a PLE map, reported by O'Connell et al.[39,35] Excitation and emission profiles extracted in the vicinity of given PL position in the PLE map were deconvoluted by using a Lorentzian shape to pinpoint S_{11} and S_{22} positions of FC12-SWNTs in *p*-xylene.

Raman Measurements. Few tens of microliters of each dispersed SWNT sample were deposited on a piranha-cleaned SiO_2/Si substrate, and residual FC12 was removed by using multiple methanol washings until no FC12-derived green PL exists in washed solution. Raman spectra were acquired using LabRam ARAmis (Horiba Jobin Yvon). Scattered light was collected via back scattering geometry using 100× objective and 600 g/mm grating. Typically, 0.7 mW laser power was used for Raman measurements to suppress unwanted SWNT damage. 632.8 and 785 nm lasers were utilized to probe HiPco and PSWNT, respectively. The Si peak (520.89 cm^{-1}) was used as an internal standard. Raman mapping was acquired by using a custom-made Raman setup with mechanical xy stage (SCAN 75 × 50, Marzhauser) and 532 nm diode-pumped solid state (DPSS) laser at 0.8 mW power, according to previously reported literature.[69] An area of 50 × 50 μm^2 containing dropcast s-PSWNT film was measured, and the pixel size is 1 × 1 μm^2.

Photoreduced FC12-PSWNT Sample Preparation. The SWNT precipitation process is facilitated by using 365 nm UV irradiation from a hand-held UV lamp for a few hours. The sample was centrifuged at 3000*g* for 2 min, and the majority of supernatant was discarded. *N*-Methyl-2-pyrrolidone (NMP) corresponding to half of the initial *p*-xylene amount was introduced into the tube, which was tip sonicated for 5 min to produce homogeneous dispersion. UV−vis−NIR absorption spectra of photoreduced FC12-PSWNT and HiPco were collected, while samples are mechanically agitated.

LC−MS Measurements. LC−MS spectra were acquired using 1260 Infinity LC/6530 and Accurate Q-TOF (Agilent Technologies). 0.1% formic acid was used to ionize molecule. FC12-depleted SWNT dispersion in *p*-xylene was first filtered with a 0.45 μm pore poly(tetrafluoroethylene) (PTFE) syringe filter to remove SWNTs, and the resulting solution was evaporated to dryness under vacuum. The resulting residue was dissolved in 3 mL of methanol, and the solution was injected into LC with a flow rate of 0.5 mL/min using a C18 reverse column. Electron spray ionization mass spectra were acquired by irradiating eluent with dual AJS ESI ion source using 4000 V energy, and ion polarity is in a positive mode.

TGA Measurements and Isolation Yield Calculation of s-PSWNTs. A mixture of 225 mg of PWNT, 225 mg of FC12, and 900 mL of *p*-xylene was used to prepare PSWNT dispersion. The sample was prepared by the above dispersion protocol, and 84.2% (or 758 mL) of supernatant centrifuged at 5000*g* was collected. The supernatant was subject to hand-held 365 nm UV irradiation overnight. The flocculated sample was filtered by a Teflon filter paper (pore size: 0.45 μm, diameter: 25 mm, PVDF, Cat. No.:HVLP02500, Millipore) and was subject to methanol washing several times to remove excess reduced FC12. The sample is further dried at 150 °C under vacuum. The final weight of SWNT film is 23.2 mg and is subject to analysis. TGA shows that about 47 wt % originates from the SWNT. Based on 47% SWNT contents in the supernatant volume, nominal 66.7% semiconductor abundance in conservative 70% PSWNT purity, the isolation yield is about 13%.

TFT Device Fabrications. Backgate TFT devices were fabricated. Sample 1 prepared by dropcasting of 5000*g* s-enriched PSWNTs: For the source and drain ohmic contact electrodes, Au/Ti (50/25 nm) was deposited on a 285 nm thick SiO_2/p^+-Si substrate (resistivity < 0.005 Ω cm) by using a DC magnetron sputtering system, while those were patterned by photolithography and lift-off process with lift-off layer (LOR 5A, MicroChem) and photoresist layer (AZ GXR-601, AZ electronic materials). An amount of 500 μL of 5000*g* of s-enriched supernatant solution was dropcast and incubated on the prepatterned substrate until solvent is removed, and the substrate was washed with methanol several times until no green PL originating from FC12 was observed by using a hand-held UV lamp. This sample was further air-annealed at 250 °C for 1 h to remove any adsorbates. s-PSWNTs were patterned by photolithography and O_2 plasma dry etching process with photoresist layer. For the dielectric layer, 50 nm of Al_2O_3 layer was deposited by an atomic layer deposition[9] system. The channel width/length were defined to be 300 μm/20 μm for our s-SWNT TFTs, and the device current−voltage (*I*−*V*) characteristics were measured using a semiconductor parameter analyzer (HP 4155C, Agilent Technologies) under ambient conditions. Using this method, 20 s-SWNT and 19 m-SWNT TFT devices have been investigated. Sample 2 prepared by dipcoating the prepatterned substrate in 30 k*g* s-PSWNTs: The channels *L*/*W* were defined with 200/20 μm. The prepatterned Si pieces were immersed into 30 k*g* s-enriched PSWNT sample for 1 h. In this time, Al_2O_3 was not deposited. The devices were subject to the similar processes applied in the sample 1. In total 19 devices are prepared in this way.

ASSOCIATED CONTENT

Supporting Information

The Supporting Information is available free of charge on the ACS Publications website at DOI: 10.1021/acsami.6b06932.

DOI: 10.1021/acsami.6b06932
ACS Appl. Mater. Interfaces 2016, 8, 23270−23280

RBM analysis of enriched samples; purity analysis based on absorption spectrum; Raman mapping analysis; the corresponding PLE maps of FC12-PSWNTs according to varying *g*-forces; stability of FC12-PSWNT sample; Raman spectra of the as-supplied PSWNT; photograph of FC12-SWNT dispersions obtained from various centrifugal forces and background-subtracted 940 nm normalized absorption spectra of Figure 3 as a function of centrifugal force; TGA of FC12, PSWNT, and FC12-PSWNT; chromatogram of photoreduced solution, and MS spectra from selected acquisition times; comparison of absorption spectra of s-enriched FC12-PSWNT, the corresponding photoreduced and redispersed sample in NMP, and commercial IsoNanotubes-S 99%; Raman mapping of s-PSWNT deposited on a Si substrate; SEM images of s-enriched PSWNT deposited on device channel; I_D-V_G transfer curves at different starting V_G without Al_2O_3 deposition; current-gate voltage transfer and output characteristics of the TFT device prepared by using m-enriched SWNTs; S_{11} and S_{22} positions of FC12-s-SWNTs dispersion in *p*-xylene, based on PLE maps; absorption-based semiconductor purity and yields of s-PSWNTs from various protocols (PDF)

AUTHOR INFORMATION

Corresponding Author

*E-mail: syju@yonsei.ac.kr.

Author Contributions

§These authors contributed equally.

Notes

The authors declare no competing financial interest.

ACKNOWLEDGMENTS

This research was supported by the Basic Science Research Program through the National Research Foundation of Korea (NRF) funded by the Ministry of Education, Science, and Technology (2014R1A1A2055572), and in part by the Yonsei University Future-Leading Research Initiative of 2014 (2014-22-0123 and 2014-22-0168). S. Im acknowledges the financial support from NRF (NRL program: Grant No. 2014R1A2A1A01004815, Nano Materials Technology Development Program: Grant No. 2012M3A7B4034985), and Brain Korea 21 Plus Program.

REFERENCES

(1) Dresselhaus, M. S.; Dresselhaus, G.; Avouris, P. *Carbon Nanotubes: Synthesis, Structure, Properties and Applications*; Springer: Berlin, 2001.

(2) Franklin, A. D.; Luisier, M.; Han, S.-J.; Tulevski, G.; Breslin, C. M.; Gignac, L.; Lundstrom, M. S.; Haensch, W. Sub-10 nm Carbon Nanotube Transistor. *Nano Lett.* **2012**, *12* (2), 758−762.

(3) Franklin, A. D. Electronics: The Road to Carbon Nanotube Transistors. *Nature* **2013**, *498* (7455), 443−444.

(4) Tanaka, T.; Jin, H.; Miyata, Y.; Fujii, S.; Suga, H.; Naitoh, Y.; Minari, T.; Miyadera, T.; Tsukagoshi, K.; Kataura, H. Simple and Scalable Gel-Based Separation of Metallic and Semiconducting Carbon Nanotubes. *Nano Lett.* **2009**, *9* (4), 1497−1500.

(5) Wang, C.; Zhang, J.; Ryu, K.; Badmaev, A.; De Arco, L. G.; Zhou, C. Wafer-Scale Fabrication of Separated Carbon Nanotube Thin-Film Transistors for Display Applications. *Nano Lett.* **2009**, *9* (12), 4285−4291.

(6) Arnold, M. S.; Zimmerman, J. D.; Renshaw, C. K.; Xu, X.; Lunt, R. R.; Austin, C. M.; Forrest, S. R. Broad Spectral Response Using Carbon Nanotube/Organic Semiconductor/C60 Photodetectors. *Nano Lett.* **2009**, *9* (9), 3354−3358.

(7) Bindl, D. J.; Wu, M.-Y.; Prehn, F. C.; Arnold, M. S. Efficiently Harvesting Excitons from Electronic Type-Controlled Semiconducting Carbon Nanotube Films. *Nano Lett.* **2011**, *11* (2), 455−460.

(8) Roberts, M. E.; LeMieux, M. C.; Bao, Z. Sorted and Aligned Single-Walled Carbon Nanotube Networks for Transistor-Based Aqueous Chemical Sensors. *ACS Nano* **2009**, *3* (10), 3287−3293.

(9) Takahashi, T.; Takei, K.; Gillies, A. G.; Fearing, R. S.; Javey, A. Carbon Nanotube Active-Matrix Backplanes for Conformal Electronics and Sensors. *Nano Lett.* **2011**, *11* (12), 5408−5413.

(10) Hammock, M. L.; Chortos, A.; Tee, B. C. K.; Tok, J. B. H.; Bao, Z. 25th Anniversary Article: The Evolution of Electronic Skin (E-Skin): A Brief History, Design Considerations, and Recent Progress. *Adv. Mater.* **2013**, *25* (42), 5997−6038.

(11) Cao, Q.; Hur, S. H.; Zhu, Z. T.; Sun, Y. G.; Wang, C. J.; Meitl, M. A.; Shim, M.; Rogers, J. A. Highly Bendable, Transparent Thin-Film Transistors That Use Carbon-Nanotube-Based Conductors and Semiconductors with Elastomeric Dielectrics. *Adv. Mater.* **2006**, *18* (3), 304−309.

(12) Sun, D.-M.; Liu, C.; Ren, W.-C.; Cheng, H.-M. A Review of Carbon Nanotube- and Graphene-Based Flexible Thin-Film Transistors. *Small* **2013**, *9* (8), 1188−1205.

(13) Rouhi, N.; Jain, D.; Burke, P. J. High-Performance Semiconducting Nanotube Inks: Progress and Prospects. *ACS Nano* **2011**, *5* (11), 8471−8487.

(14) Xu, F.; Wu, M.-Y.; Safron, N. S.; Roy, S. S.; Jacobberger, R. M.; Bindl, D. J.; Seo, J.-H.; Chang, T.-H.; Ma, Z.; Arnold, M. S. Highly Stretchable Carbon Nanotube Transistors with Ion Gel Gate Dielectrics. *Nano Lett.* **2014**, *14* (2), 682−686.

(15) Tour, J. M. Materials Chemistry: Seeds of Selective Nanotube Growth. *Nature* **2014**, *512* (7512), 30−31.

(16) Collins, P. G.; Arnold, M. S.; Avouris, P. Engineering Carbon Nanotubes and Nanotube Circuits Using Electrical Breakdown. *Science* **2001**, *292* (5517), 706−709.

(17) Jin, S. H.; Dunham, S. N.; Song, J.; Xie, X.; Kim, J.-h.; Lu, C.; Islam, A.; Du, F.; Kim, J.; Felts, J.; Li, Y.; Xiong, F.; Wahab, M. A.; Menon, M.; Cho, E.; Grosse, K. L.; Lee, D. J.; Chung, H. U.; Pop, E.; Alam, M. A.; King, W. P.; Huang, Y.; Rogers, J. A. Using Nanoscale Thermocapillary Flows to Create Arrays of Purely Semiconducting Single-Walled Carbon Nanotubes. *Nat. Nanotechnol.* **2013**, *8* (5), 347−355.

(18) Xie, X.; Jin, S. H.; Wahab, M. A.; Islam, A. E.; Zhang, C.; Du, F.; Seabron, E.; Lu, T.; Dunham, S. N.; Cheong, H. I.; Tu, Y.-C.; Guo, Z.; Chung, H. U.; Li, Y.; Liu, Y.; Lee, J.-H.; Song, J.; Huang, Y.; Alam, M. A.; Wilson, W. L.; Rogers, J. A. Microwave Purification of Large-Area Horizontally Aligned Arrays of Single-Walled Carbon Nanotubes. *Nat. Commun.* **2014**, *5*, 5332.

(19) Zheng, M.; Jagota, A.; Semke, E. D.; Diner, B. A.; McLean, R. S.; Lustig, S. R.; Richardson, R. E.; Tassi, N. G. DNA-Assisted Dispersion and Separation of Carbon Nanotubes. *Nat. Mater.* **2003**, *2* (5), 338−342.

(20) Liu, H.; Nishide, D.; Tanaka, T.; Kataura, H. Large-Scale Single-Chirality Separation of Single-Wall Carbon Nanotubes by Simple Gel Chromatography. *Nat. Commun.* **2011**, *2*, 309.

(21) Feng, Y.; Miyata, Y.; Matsuishi, K.; Kataura, H. High-Efficiency Separation of Single-Wall Carbon Nanotubes by Self-Generated Density Gradient Ultracentrifugation. *J. Phys. Chem. C* **2011**, *115* (5), 1752−1756.

(22) Arnold, M. S.; Green, A. A.; Hulvat, J. F.; Stupp, S. I.; Hersam, M. C. Sorting Carbon Nanotubes by Electronic Structure using Density Differentiation. *Nat. Nanotechnol.* **2006**, *1* (1), 60−65.

(23) Antaris, A. L.; Seo, J.-W. T.; Green, A. A.; Hersam, M. C. Sorting Single-Walled Carbon Nanotubes by Electronic Type Using Nonionic, Biocompatible Block Copolymers. *ACS Nano* **2010**, *4* (8), 4725−4732.

(24) Khripin, C. Y.; Fagan, J. A.; Zheng, M. Spontaneous Partition of Carbon Nanotubes in Polymer-Modified Aqueous Phases. *J. Am. Chem. Soc.* **2013**, *135* (18), 6822−6825.

DOI: 10.1021/acsami.6b06932
ACS Appl. Mater. Interfaces 2016, 8, 23270−23280

(25) Fagan, J. A.; Hároz, E. H.; Ihly, R.; Gui, H.; Blackburn, J. L.; Simpson, J. R.; Lam, S.; Hight Walker, A. R.; Doorn, S. K.; Zheng, M. Isolation of > 1 nm Diameter Single-Wall Carbon Nanotube Species Using Aqueous Two-Phase Extraction. *ACS Nano* **2015**, *9* (5), 5377−5390.
(26) Nish, A.; Hwang, J.-Y.; Doig, J.; Nicholas, R. J. Highly Selective Dispersion of Single-Walled Carbon Nanotubes Using Aromatic Polymers. *Nat. Nanotechnol.* **2007**, *2* (10), 640−646.
(27) Wang, H.; Mei, J.; Liu, P.; Schmidt, K.; Jiménez-Osés, G.; Osuna, S.; Fang, L.; Tassone, C. J.; Zoombelt, A. P.; Sokolov, A. N.; Houk, K. N.; Toney, M. F.; Bao, Z. Scalable and Selective Dispersion of Semiconducting Arc-Discharged Carbon Nanotubes by Dithiafulvalene/Thiophene Copolymers for Thin Film Transistors. *ACS Nano* **2013**, *7* (3), 2659−2668.
(28) Sundramoorthy, A. K.; Mesgari, S.; Wang, J.; Kumar, R.; Sk, M. A.; Yeap, S. H.; Zhang, Q.; Sze, S. K.; Lim, K. H.; Chan-Park, M. B. Scalable and Effective Enrichment of Semiconducting Single-Walled Carbon Nanotubes by a Dual Selective Naphthalene-Based Azo Dispersant. *J. Am. Chem. Soc.* **2013**, *135* (15), 5569−5581.
(29) Mistry, K. S.; Larsen, B. A.; Blackburn, J. L. High-Yield Dispersions of Large-Diameter Semiconducting Single-Walled Carbon Nanotubes with Tunable Narrow Chirality Distributions. *ACS Nano* **2013**, *7* (3), 2231−2239.
(30) Tu, X.; Manohar, S.; Jagota, A.; Zheng, M. DNA Sequence Motifs for Structure-Specific Recognition and Separation of Carbon Nanotubes. *Nature* **2009**, *460* (7252), 250−253.
(31) Ghosh, S.; Bachilo, S. M.; Weisman, R. B. Advanced Sorting of Single-Walled Carbon Nanotubes by Nonlinear Density-Gradient Ultracentrifugation. *Nat. Nanotechnol.* **2010**, *5* (6), 443−450.
(32) Hennrich, F.; Li, W.; Fischer, R.; Lebedkin, S.; Krupke, R.; Kappes, M. M. Length-Sorted, Large-Diameter, Polyfluorene-Wrapped Semiconducting Single-Walled Carbon Nanotubes for High-Density, Short-Channel Transistors. *ACS Nano* **2016**, *10* (2), 1888−1895.
(33) Ding, J.; Li, Z.; Lefebvre, J.; Cheng, F.; Dubey, G.; Zou, S.; Finnie, P.; Hrdina, A.; Scoles, L.; Lopinski, G. P.; Kingston, C. T.; Simard, B.; Malenfant, P. R. L. Enrichment of Large-Diameter Semiconducting SWCNTs by Polyfluorene Extraction for High Network Density Thin Film Transistors. *Nanoscale* **2014**, *6* (4), 2328−2339.
(34) Gui, H.; Streit, J. K.; Fagan, J. A.; Hight Walker, A. R.; Zhou, C.; Zheng, M. Redox Sorting of Carbon Nanotubes. *Nano Lett.* **2015**, *15* (3), 1642−1646.
(35) Ju, S.-Y.; Doll, J.; Sharma, I.; Papadimitrakopoulos, F. Selection of Carbon Nanotubes with Specific Chiralities using Helical Assemblies of Flavin Mononucleotide. *Nat. Nanotechnol.* **2008**, *3* (6), 356−362.
(36) Ju, S.-Y.; Kopcha, W. P.; Papadimitrakopoulos, F. Brightly Fluorescent Single-Walled Carbon Nanotubes via an Oxygen-Excluding Surfactant Organization. *Science* **2009**, *323* (5919), 1319−1323.
(37) Kato, Y.; Fukuzawa, M.; Toshimitsu, F.; Nakashima, N. Separation of Semiconducting Single-Walled Carbon Nanotubes Using a Flavin Compound. *Chem. Lett.* **2015**, *44* (4), 566−567.
(38) Franklin, A. D. Nanomaterials in Transistors: From High-Performance to Thin-Film Applications. *Science* **2015**, *349* (6249), aab2750.
(39) O'Connell, M. J.; Bachilo, S. M.; Huffman, C. B.; Moore, V. C.; Strano, M. S.; Haroz, E. H.; Rialon, K. L.; Boul, P. J.; Noon, W. H.; Kittrell, C.; Ma, J.; Hauge, R. H.; Weisman, R. B.; Smalley, R. E. Band Gap Fluorescence from Individual Single-Walled Carbon Nanotubes. *Science* **2002**, *297* (5581), 593−596.
(40) Hennrich, F.; Krupke, R.; Lebedkin, S.; Arnold, K.; Fischer, R.; Resasco, D. E.; Kappes, M. M. Raman Spectroscopy of Individual Single-Walled Carbon Nanotubes from Various Sources. *J. Phys. Chem. B* **2005**, *109* (21), 10567−10573.
(41) Bachilo, S. M.; Strano, M. S.; Kittrell, C.; Hauge, R. H.; Smalley, R. E.; Weisman, R. B. Structure-Assigned Optical Spectra of Single-Walled Carbon Nanotubes. *Science* **2002**, *298* (5602), 2361−2366.
(42) Liu, K.; Hong, X.; Choi, S.; Jin, C.; Capaz, R. B.; Kim, J.; Wang, W.; Bai, X.; Louie, S. G.; Wang, E.; Wang, F. Systematic Determination of Absolute Absorption Cross-Section of Individual Carbon Nanotubes. *Proc. Natl. Acad. Sci. U. S. A.* **2014**, *111* (21), 7564−7569.
(43) Kataura, H.; Kumazawa, Y.; Maniwa, Y.; Umezu, I.; Suzuki, S.; Ohtsuka, Y.; Achiba, Y. Optical Properties of Single-Wall Carbon Nanotubes. *Synth. Met.* **1999**, *103* (1−3), 2555−2558.
(44) Fantini, C.; Jorio, A.; Souza, M.; Strano, M. S.; Dresselhaus, M. S.; Pimenta, M. A. Optical Transition Energies for Carbon Nanotubes from Resonant Raman Spectroscopy: Environment and Temperature Effects. *Phys. Rev. Lett.* **2004**, *93* (14), 147406.
(45) Strano, M. S. Probing Chiral Selective Reactions Using a Revised Kataura Plot for the Interpretation of Single-Walled Carbon Nanotube Spectroscopy. *J. Am. Chem. Soc.* **2003**, *125* (51), 16148−16153.
(46) Brown, S. D. M.; Jorio, A.; Corio, P.; Dresselhaus, M. S.; Dresselhaus, G.; Saito, R.; Kneipp, K. Origin of the Breit-Wigner-Fano Lineshape of the Tangential G-Band Feature of Metallic Carbon Nanotubes. *Phys. Rev. B: Condens. Matter Mater. Phys.* **2001**, *63* (15), 155414.
(47) Ogunro, O. O.; Wang, X.-Q. Quantum Electronic Stability in Selective Enrichment of Carbon Nanotubes. *Nano Lett.* **2009**, *9* (3), 1034−1038.
(48) Yoon, W.; Lee, Y.; Jang, H.; Jang, M.; Kim, J. S.; Lee, H. S.; Im, S.; Boo, D. W.; Park, J.; Ju, S.-Y. Graphene Nanoribbons Formed by a Sonochemical Graphene Unzipping Using Flavin Mononucleotide as a Template. *Carbon* **2015**, *81*, 629−638.
(49) Itkis, M. E.; Perea, D. E.; Jung, R.; Niyogi, S.; Haddon, R. C. Comparison of Analytical Techniques for Purity Evaluation of Single-Walled Carbon Nanotubes. *J. Am. Chem. Soc.* **2005**, *127* (10), 3439−3448.
(50) Schießl, S. P.; Fröhlich, N.; Held, M.; Gannott, F.; Schweiger, M.; Forster, M.; Scherf, U.; Zaumseil, J. Polymer-Sorted Semiconducting Carbon Nanotube Networks for High-Performance Ambipolar Field-Effect Transistors. *ACS Appl. Mater. Interfaces* **2015**, *7* (1), 682−689.
(51) Wang, J.; Nguyen, T. D.; Cao, Q.; Wang, Y.; Tan, M. Y. C.; Chan-Park, M. B. Selective Surface Charge Sign Reversal on Metallic Carbon Nanotubes for Facile Ultrahigh Purity Nanotube Sorting. *ACS Nano* **2016**, *10* (3), 3222−3232.
(52) Strano, M. S.; Dyke, C. A.; Usrey, M. L.; Barone, P. W.; Allen, M. J.; Shan, H.; Kittrell, C.; Hauge, R. H.; Tour, J. M.; Smalley, R. E. Electronic Structure Control of Single-Walled Carbon Nanotube Functionalization. *Science* **2003**, *301* (5639), 1519−1522.
(53) Nish, A.; Hwang, J.-Y.; Doig, J.; Nicholas, R. J. Direct Spectroscopic Evidence of Energy Rransfer from Photo-Excited Semiconducting Polymers to Single-Walled Carbon Nanotubes. *Nanotechnology* **2008**, *19* (9), 095603.
(54) Yanagi, K.; Iakoubovskii, K.; Matsui, H.; Matsuzaki, H.; Okamoto, H.; Miyata, Y.; Maniwa, Y.; Kazaoui, S.; Minami, N.; Kataura, H. Photosensitive Function of Encapsulated Dye in Carbon Nanotubes. *J. Am. Chem. Soc.* **2007**, *129* (16), 4992−4997.
(55) Sun, M.; Moore, T. A.; Song, P.-S. Molecular Luminescence Studies of Flavines. I. Excited States of Flavines. *J. Am. Chem. Soc.* **1972**, *94* (5), 1730−1740.
(56) Hughes, M. E.; Brandin, E.; Golovchenko, J. A. Optical Absorption of DNA−Carbon Nanotube Structures. *Nano Lett.* **2007**, *7* (5), 1191−1194.
(57) Freer, A.; Prince, S.; Sauer, K.; Papiz, M.; Lawless, A. H.; McDermott, G.; Cogdell, R.; Isaacs, N. W. Pigment−Pigment Interactions and Energy Transfer in the Antenna Complex of the Photosynthetic Bacterium Rhodopseudomonas Acidophila. *Structure* **1996**, *4* (4), 449−462.
(58) Birks, J. B.; Lumb, M. D.; Munro, I. H. 'Excimer' Fluorescence. V. Influence of Solvent Viscosity and Temperature. *Proc. R. Soc. London, Ser. A* **1964**, *280* (1381), 289−297.
(59) Sichula, V.; Kucheryavy, P.; Khatmullin, R.; Hu, Y.; Mirzakulova, E.; Vyas, S.; Manzer, S. F.; Hadad, C. M.; Glusac, K. D. Electronic Properties of N(5)-Ethyl Flavinium Ion. *J. Phys. Chem. A* **2010**, *114* (46), 12138−12147.
(60) Suzuki, S.; Watanabe, Y.; Homma, Y.; Fukuba, S.-y.; Heun, S.; Locatelli, A. Work Functions of Individual Single-Walled Carbon Nanotubes. *Appl. Phys. Lett.* **2004**, *85* (1), 127−129.
(61) Lin, C. S.; Zhang, R. Q.; Niehaus, T. A.; Frauenheim, T. Geometric and Electronic Structures of Carbon Nanotubes Adsorbed

DOI: 10.1021/acsami.6b06932
ACS Appl. Mater. Interfaces 2016, 8, 23270−23280

with Flavin Adenine Dinucleotide: A Theoretical Study. *J. Phys. Chem. C* **2007**, *111* (11), 4069−4073.
(62) Guiseppi-Elie, A.; Lei, C.; Baughman, R. H. Direct Electron Transfer of Glucose Oxidase on Carbon Nanotubes. *Nanotechnology* **2002**, *13* (5), 559.
(63) Song, S. H.; Dick, B.; Penzkofer, A. Photo-Induced Reduction of Flavin Mononucleotide in Aqueous Solutions. *Chem. Phys.* **2007**, *332* (1), 55−65.
(64) Zhang, W.; Zhang, M.; Zhu, W.; Zhou, Y.; Wanduragala, S.; Rewinkel, D.; Tanner, J. J.; Becker, D. F. Redox-Induced Changes in Flavin Structure and Roles of Flavin N(5) and the Ribityl 2′-OH Group in Regulating PutA-Membrane Binding. *Biochemistry* **2007**, *46* (2), 483−491.
(65) Dixon, D. A.; Lindner, D. L.; Branchaud, B.; Lipscomb, W. N. Conformations and Electronic Structures of Oxidized and Reduced Isoalloxazine. *Biochemistry* **1979**, *18* (26), 5770−5775.
(66) Ju, S.-Y.; Papadimitrakopoulos, F. Synthesis and Redox Behavior of Flavin Mononucleotide-Functionalized Single-Walled Carbon Nanotubes. *J. Am. Chem. Soc.* **2007**, *130* (2), 655−664.
(67) Sim, J.; Oh, H.; Koo, E.; Ju, S.-Y. Effect of Tight Flavin Mononucleotide Wrapping and Its Binding Affinity on Carbon Nanotube Covalent Reactivities. *Phys. Chem. Chem. Phys.* **2013**, *15* (44), 19169−19179.
(68) Nikolaev, P.; Bronikowski, M. J.; Bradley, R. K.; Rohmund, F.; Colbert, D. T.; Smith, K. A.; Smalley, R. E. Gas-Phase Catalytic Growth of Single-Walled Carbon Nanotubes from Carbon Monoxide. *Chem. Phys. Lett.* **1999**, *313* (1−2), 91−97.
(69) Koo, E.; Ju, S.-Y. Role of Residual Polymer on Chemical Vapor Grown Graphene by Raman Spectroscopy. *Carbon* **2015**, *86*, 318−324.

DOI: 10.1021/acsami.6b06932
ACS Appl. Mater. Interfaces 2016, 8, 23270−23280

Supporting Information for

Selective Dispersion of Highly Pure Large-Diameter Semiconducting Carbon Nanotubes by a Flavin for Thin Film Transistors

Minsuk Park,[1,‡] Somin Kim,[1,‡] Hyeokjae Kwon,[2,‡] Sukhyun Hong,[1] Seongil Im,[2]

and Sang-Yong Ju [1,]*

[1]Department of Chemistry and [2]Department of Physics, Yonsei University, Seoul 03722, Republic of Korea

* E-mail address: syju@yonsei.ac.kr

‡ Equally contributed to this work

RBM analysis of enriched samples

After careful calibration with respect to Si peak at 520.89 cm^{-1}, Raman RBM frequency (ω_{RBM}) analysis on separated PSWNT and HiPco samples were conducted. Assuming the *d* distribution as Gaussian profile, one can expect that peak intensity of resonating SWNTs would decrease when deviations from the average *d* occurs. PSWNT has a median *d* at 1.35 nm with ± 0.4 nm distribution. With 785 nm excitation, the observed ω_{RBM} peak from the supernatant of FC12-PSWNT are 161.5, 190.5, 205.6, 216.4, and 225.0 cm^{-1}. Using the empirical diameter-ω_{RBM} relationship (i.e., semiconducting: $\omega_{RBM} = 223/d + 10$, metallic: $\omega_{RBM} = 218/d + 17$),[S1-2] one can assign m- and s-PSWNTs for a given PSWNT. The 161.5 and 190.5 cm^{-1} peaks derive from m-SWNTs whereas the 205.6, 216.4 and 225.0 cm^{-1} peaks originate from s-SWNTs. By comparison of underlying area, s- and m-enrichments of PSWNT are determined to be 95 and 78%, respectively. However, it needs to be pointed out that resonating m-SWNTs are situated at near median diameter (1.35 nm or 176 cm^{-1}) and, therefore, appear to have much greater population than those of s-SWNTs, leading to overestimation of the metallic content. Similarly, HiPco has *d* distribution ranging from 0.65 to 1.35 nm, centered at 1.0 nm.[3] With 632.8 nm laser (or 1.96 eV), observed RBM peaks (ω_{RBM}) from supernatant are 195.1, 218.5, 256.3, and 285.1 cm^{-1}. Among those peaks, the 195.1 and 218.5 cm^{-1} peaks originate from m-SWNTs, and the 256.3 and 285.1 cm^{-1} peaks derive from s-SWNTs. Because the observed s- and m-SWNTs are distributed equally from the median *d* line, one can assume that each electronic structure would be excited with similar probability using resonating laser windows (i.e., ±0.1 eV). By calculating each s- and m-area of respective supernatant and precipitate, the number-averaged s- and m-SWNT enrichments of HiPco are determined to be 76 and 61%, respectively.

Purity analysis based on absorption spectrum

Absorption spectra containing distinct S_{22} and M_{11} peak regions were used to determine purity of enriched s-PSWNTs, according to previously reported literature.[S4-8] SDS-dispersed PSWNT was utilized as a reference having 1 part of m- and 2 part of s-SWNTs. In the case of SDS-PSWNTs dispersion, the summated peak areas of background-subtracted m- (570-750 nm) and s- (750-1200 nm) absorption region are 1 and 8.74, respectively, which are tabulated in Table S2. s-/m- peak ratio of FC12-PSWNTs with varying centrifugal speed in Figure 3 are 250.8, 349.5, 1152, and 1218 for 5, 10, 20, and 30 k*g* samples. Those s-/m- peak area ratio was divided by SDS-based normalization factor (i.e., 8.74) to produce s-/m- abundance ratio and s-PSWNT purity. The results are summarized in Table S2. Moreover, we added absorption spectra of a commercially available 99% enriched s-SWNT with similar diameter, as shown in Figure S7.

Raman mapping analysis

Unfortunately, the broad *d* distribution of PSWNT hampers us to estimate s- and m-purity based on G^+ and G^- band intensities proposed by Finnie *et al*.[S9] Instead, in order to verify a spatial homogeneity of purity of the deposited s-PSWNT on a Si substrate, Raman mapping probed by 532 nm was acquired. This measurement allows us to probe smaller *d* m- and larger *d* s-PSWNTs originating from M_{11} and S_{33} transitions, complementary to *d* information obtained by 785 nm excitation. Figure S8 displays Raman data extracted from Raman mapping whose size is 50×50 μm^2 with pixel size of 1×1 μm^2. Overlaid 2500 RBM spectra displays no particular RBM signal originating from m-PSWNT, as indicated by dotted line based on the above d-ω_{RBM} relationship. In addition, G band spectra exhibit absent BWF shape originating from m-PSWNT. In addition, summated RBM intensity shows that RBM intensity from s-PSWNTs is dominant as compared to

that from m-PSWNTs. It is noteworthy that majority of the m-PSWNT signal originates from residual peak tails from s-PSWNT. This suggests that the enriched sample possesses not only high purity, but also have spatial electronic homogeneity. Intensity map from G^+ and G^- bands displays that there is no deviation in the intensity pattern, suggesting the absence of BWF peak originating from m-PSWNTs.

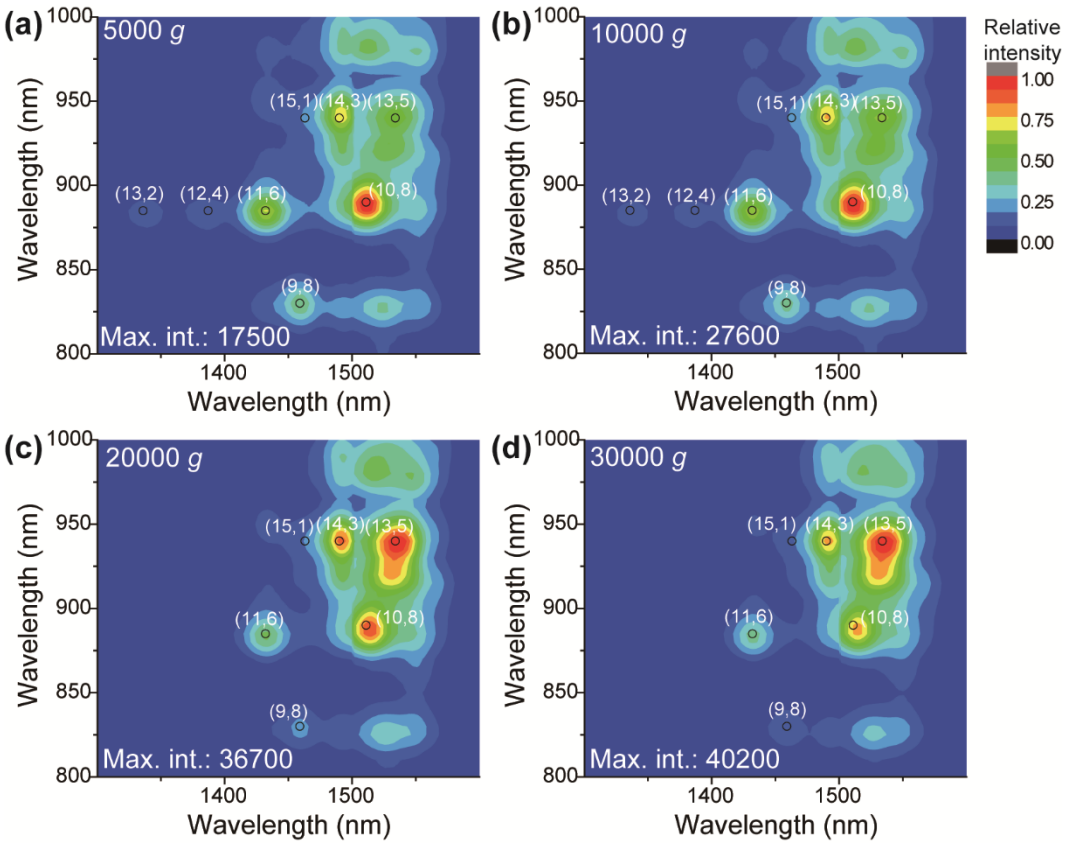

Figure S1. (a - d) The corresponding PLE maps of FC12-PSWNTs according to varying *g*-forces.

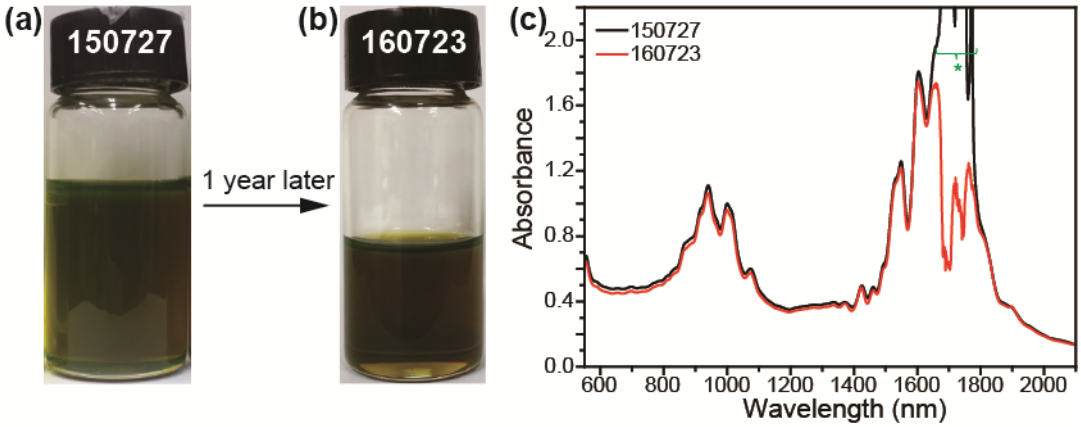

Figure S2. Stability of FC12-PSWNT sample. Photographs of (a) the initial and (b) one year old sample. The reduction in the dispersion is owing to a measurement. (c) The corresponding absorption spectra. An asterisk indicates the absorption attributed to the solvent.

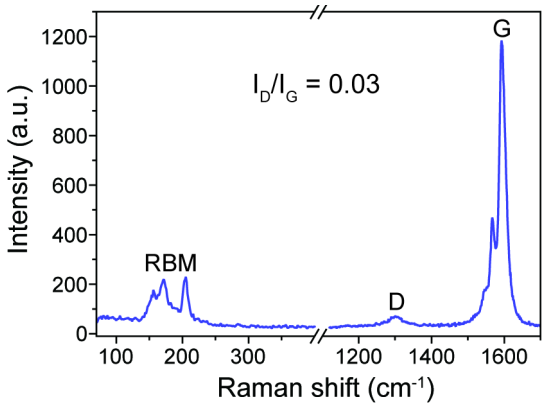

Figure S3. Raman spectra of the as-supplied PSWNT. Laser excitation: 785 nm.

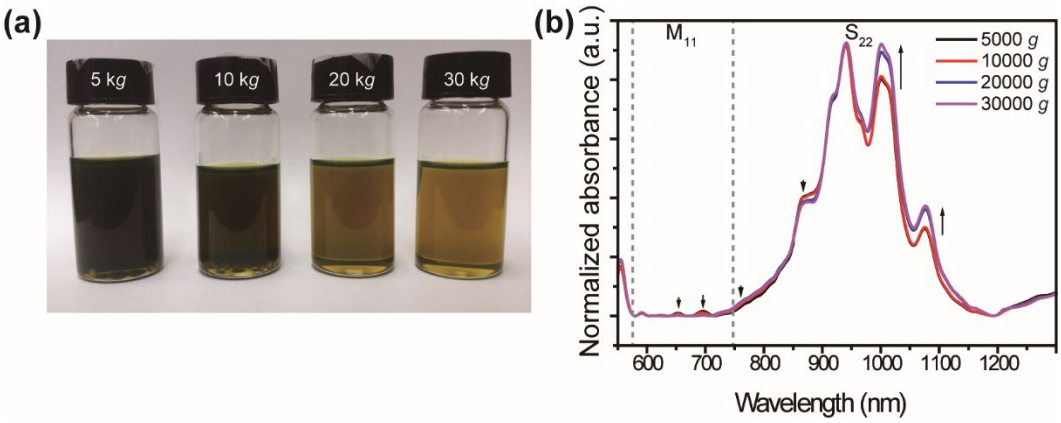

Figure S4. Background-subtracted 940-nm normalized absorption spectra of Figure 3 as a function of centrifugal force. (a) Photograph of FC12-SWNT dispersions obtained from various centrifugal forces. (b) The corresponding normalized absorption spectra based on 940 nm band.

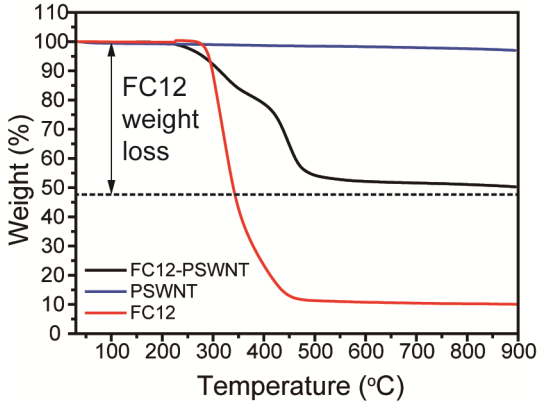

Figure S5. TGA of FC12, PSWNT, and excess FC12 removed, photoreduced FC12-PSWNT.

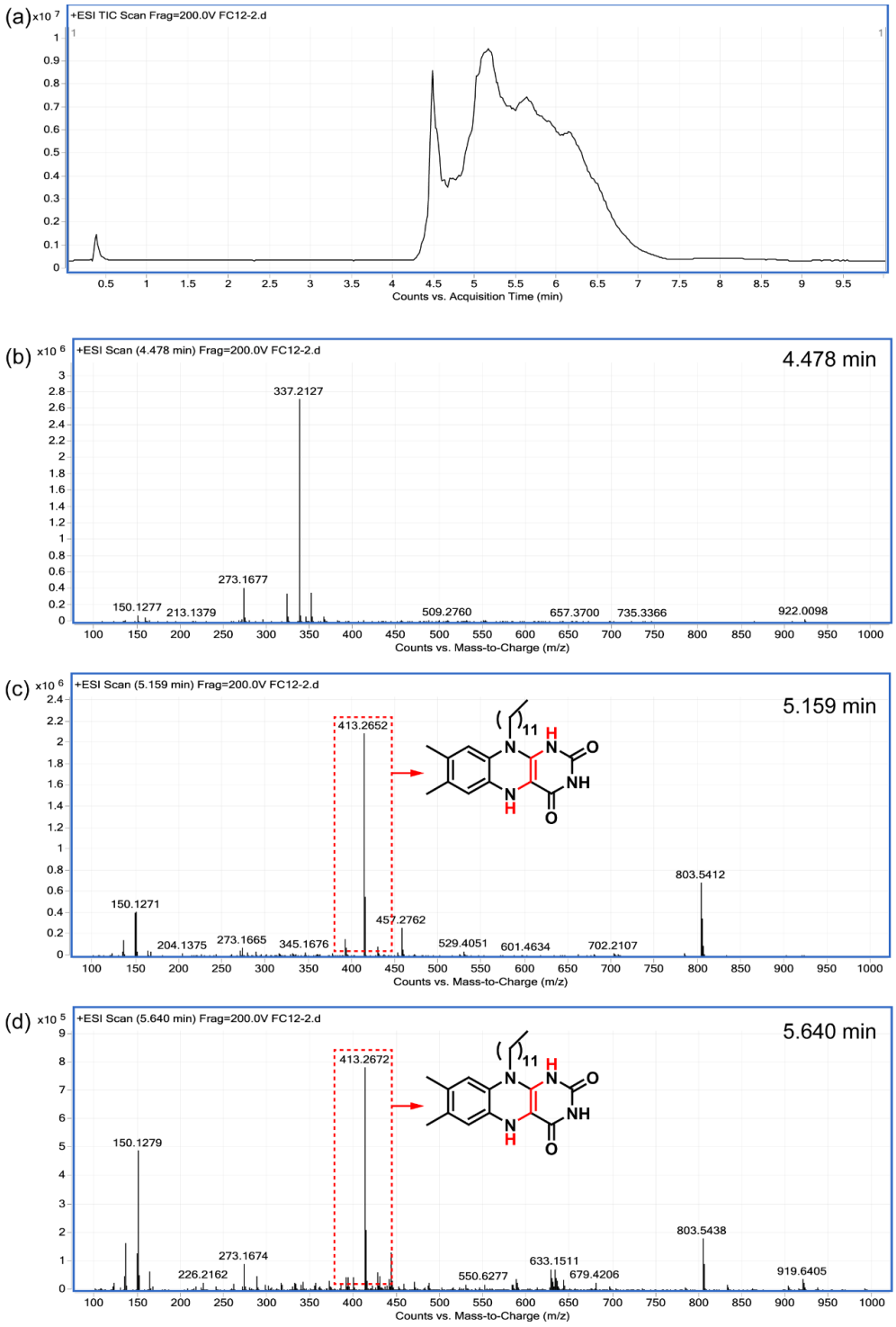

Figure S6. (a) Chromatogram of photoreduced solution, and (b-d) MS spectra from selected acquisition times.

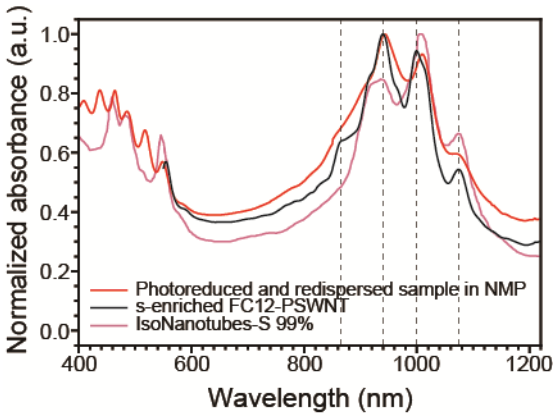

Figure S7. Comparison of absorption spectra of s-enriched FC12-PSWNT (black) and the corresponding photoreduced and redispersed sample in NMP (red), as compared to that of commercial IsoNanotubes-S 99%.

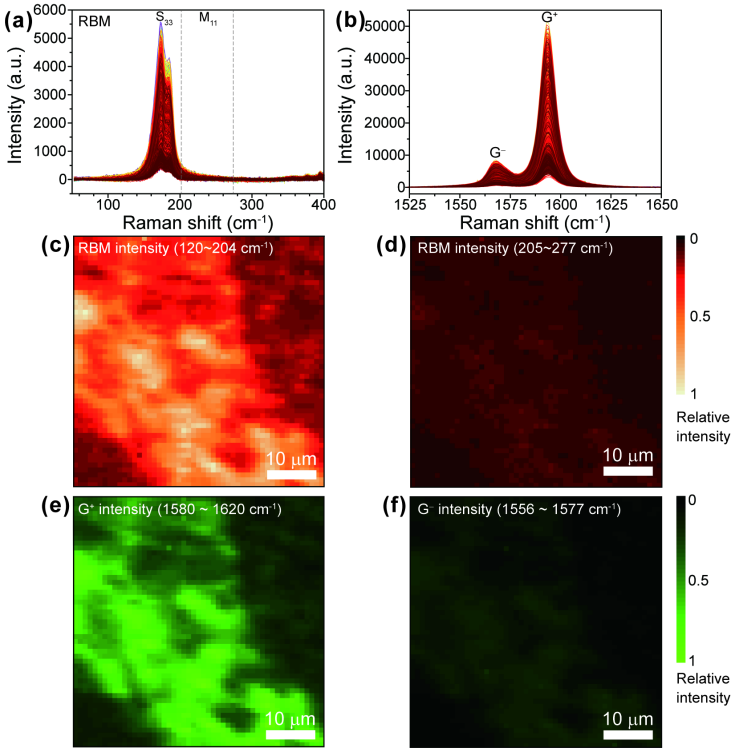

Figure S8. Raman mapping of s-PSWNT deposited on a Si substrate. (a) RBM and (b) G band spectra from 2500 different points. Summated intensities of RBM regions of (c) 120-204 cm^{-1} from s-PSWNTs and (d) 205-277 cm^{-1} from m-PSWNTs. Summated intensities of (e) G^+ (1580-1620 cm^{-1}) and (f) G^- (1556-1577 cm^{-1}) bands.

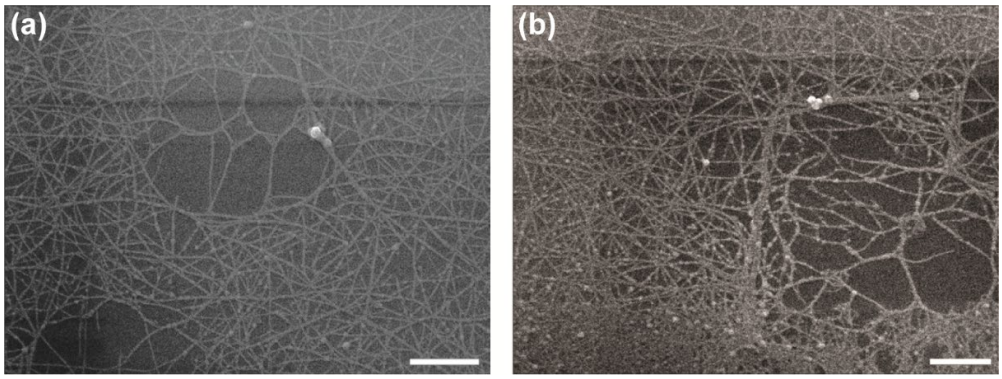

Figure S9. (a – b) SEM images of s-enriched PSWNT deposited on device channel. Scale bar: 1 μm.

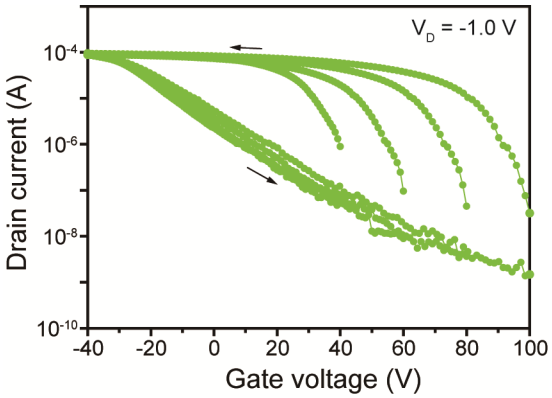

Figure S10. I_D-V_G transfer curves at different starting V_G without Al_2O_3 deposition.

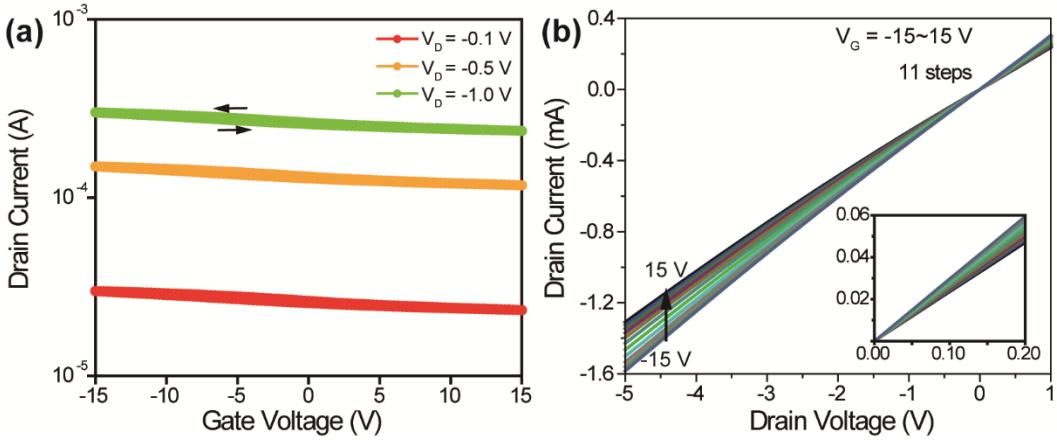

Figure S11. (a) Current-gate voltage transfer and (b) output characteristics of the TFT device prepared by using m-enriched SWNTs.

Table S1. S_{11} and S_{22} positions of FC12- s-SWNTs dispersion in *p*-xylene, based on PLE maps. SWNT diameter was calculated from 1.44 Å C-C bond length.

Assignment (*n, m*)	Diameter (nm)	Optical transitions		Observed (*n*,*m*)	
		S_{11} (nm)	S_{22} (nm)	HiPco	PSWNTs
(6,5)	0.76	986.7	581.9	○	
(8,3)	0.78	980.8	673.8	○	
(7,5)	0.83	1044.9	656.9	○	
(8,4)	0.84	1124.6	605.8	○	
(10,2)	0.88	1069.0	751.2	○	
(7,6)	0.90	1147.4	662.0	○	
(9,4)	0.92	1118.6	736.3	○	
(11,1)	0.92	1303.3	624.3	○	
(10,3)	0.94	1273.9	645.4	○	
(8,6)	0.97	1205.7	734.0	○	
(9,5)	0.98	1269.2	689.5	○	
(11,3)	1.01	1217.6	823.4	○	
(13,0)	1.03	1418.3	687.8	○	
(8,7)	1.03	1308.1	741.6	○	
(10,5)	1.05	1280.9	823.8	○	
(11,4)	1.07	1413.1	729.9	○	
(9,7)	1.10	1369.6	825.6	○	
(10,6)	1.11	1420.1	765.8	○	
(13,2)	1.12	1334.6	883.4	○	○
(12,4)	1.15	1383.4	883.1	○	○
(9,8)	1.17	1458.7	829.4	○	○
(11,6)	1.19	1432.4	884.9	○	○
(15,1)	1.23	1463	940	○	○
(10,8)	1.24	1512.7	889.1	○	○
(14,3)	1.25	1489.8	941.9	○	○
(13,5)	1.28	1534.6	936.6	○	○

Table S2. Absorption-based semiconductor purity and yields of s-PSWNTs from various protocols.

Sample		Peak area ratio of S_{22}/ M_{11}	Abundance ratio of s-/m-PSWNT	s-PSWNT purity (%)	s-PSWNT yield (%)
FC12-PSWNT	5000 *g*	250.8	57.38	98.28	13
	10000 *g*	349.5	79.97	98.76	10.4
	20000 *g*	1152	263.7	99.62	4.8
	30000 *g*	1218	278.7	99.64	3.9
SDS-PSWNT		8.741	2.000	66.67	

Cited references

(S1) Hennrich, F.; Krupke, R.; Lebedkin, S.; Arnold, K.; Fischer, R.; Resasco, D. E.; Kappes, M. M., Raman Spectroscopy of Individual Single-Walled Carbon Nanotubes from Various Sources. *J. Phys. Chem. B* **2005,** *109* (21), 10567-10573.

(S2) Bachilo, S. M.; Strano, M. S.; Kittrell, C.; Hauge, R. H.; Smalley, R. E.; Weisman, R. B., Structure-Assigned Optical Spectra of Single-Walled Carbon Nanotubes. *Science* **2002,** *298* (5602), 2361-2366.

(S3) Nikolaev, P.; Bronikowski, M. J.; Bradley, R. K.; Rohmund, F.; Colbert, D. T.; Smith, K. A.; Smalley, R. E., Gas-Phase Catalytic Growth of Single-Walled Carbon Nanotubes from Carbon Monoxide. *Chem. Phys. Lett.* **1999,** *313* (1–2), 91-97.

(S4) Itkis, M. E.; Perea, D. E.; Jung, R.; Niyogi, S.; Haddon, R. C., Comparison of Analytical Techniques for Purity Evaluation of Single-Walled Carbon Nanotubes. *J. Phys. Soc. Japan* **2005,** *127* (10), 3439-3448.

(S5) Tanaka, T.; Jin, H.; Miyata, Y.; Fujii, S.; Suga, H.; Naitoh, Y.; Minari, T.; Miyadera, T.; Tsukagoshi, K.; Kataura, H., Simple and Scalable Gel-Based Separation of Metallic and Semiconducting Carbon Nanotubes. *Nano Lett.* **2009,** *9* (4), 1497-1500.

(S6) Antaris, A. L.; Seo, J.-W. T.; Green, A. A.; Hersam, M. C., Sorting Single-Walled Carbon Nanotubes by Electronic Type Using Nonionic, Biocompatible Block Copolymers. *ACS Nano* **2010,** *4* (8), 4725-4732.

(S7) Sundramoorthy, A. K.; Mesgari, S.; Wang, J.; Kumar, R.; Sk, M. A.; Yeap, S. H.; Zhang, Q.; Sze, S. K.; Lim, K. H.; Chan-Park, M. B., Scalable and Effective Enrichment of Semiconducting Single-Walled Carbon Nanotubes by a Dual Selective Naphthalene-Based Azo Dispersant. *J. Am. Chem. Soc.* **2013,** *135* (15), 5569-5581.

(S8) Mistry, K. S.; Larsen, B. A.; Blackburn, J. L., High-Yield Dispersions of Large-Diameter Semiconducting Single-Walled Carbon Nanotubes with Tunable Narrow Chirality Distributions. *ACS Nano* **2013,** *7* (3), 2231-2239.

(S9) Finnie, P.; Ding, J.; Li, Z.; Kingston, C. T., Assessment of the Metallicity of Single-Wall Carbon Nanotube Ensembles at High Purities. *J. Phys. Chem. C* **2014,** *118* (51), 30127-30138.